MODELING, SIMULATION, AND MITIGATION OF THE IMPACTS OF THE LATE TIME (E3) HIGH-ALTITUDE ELECTROMAGNETIC PULSE ON POWER SYSTEMS

BY

TREVOR HUTCHINS

DISSERTATION

Submitted in partial fulfillment of the requirements
for the degree of Doctor of Philosophy in Electrical and Computer Engineering
in the Graduate College of the
University of Illinois at Urbana-Champaign, 2016

Urbana, Illinois

Doctoral Committee:

Professor Thomas J. Overbye, Chair
Professor Peter W. Sauer
Professor Jonathan J. Makela
Associate Professor Alejandro Dominguez-Garcia
Assistant Professor Hao Zhu

ABSTRACT

High impact, low frequency (HILF) events are a growing concern in civilian and military domains. Two HILF events of concern are geomagnetic disturbances (GMDs), also known as geomagnetic storms, and high-altitude electromagnetic pulses (HEMPs). These two events have the potential to cripple electric grids and damage electronics. The study of HEMPs and their effects on the electric grid have often been associated with the effects of GMDs. The quicker rise-times and larger magnitudes of electric fields induced by HEMPs, as compared to GMDs, can significantly impact the large disturbance voltage stability of the power system. This dissertation presents a methodology for integrating HEMP impacts into power system transient stability assessments. The beginning simulations of this dissertation use relatively simple models to model the dynamics in the power system. As the dissertation progresses, more detailed and accurate models are incorporated in order to capture the most realistic response as possible. Various test cases were created in order to simulate the effects of HEMP on power systems as a part of this research. The research and transient stability studies performed in this dissertation indicate that second to minute long dynamics are crucial when simulating the impacts of HEMPs on power systems in order to gain an accurate understanding of the impacts. This research created and determined power system

models appropriate for HEMP analysis, and ultimately serves to inform power system engineers about what models are most suitable in use for HEMP analysis on the electric grid.

ACKNOWLEDGMENTS

I would like to thank my advisor, Thomas J. Overbye, for his patience and mentorship throughout my graduate academic career. He has taught me a great deal about what it means to be a good teacher, professor, advisor, and Christian. I would also like to acknowledge my funding sources, the Illinois Center for a Smart Electric Grid (ICSEG) and the UIUC Grainger Fellowship Program.

Without naming names, there were several peers that were instrumental to my success as a graduate student at UIUC. It was a pleasure to study, suffer, celebrate, compete, and grow alongside such bright and motivated people. A special thanks to the Saturday Morning Brunch (SMB) crew.

I would like to extend a special thank you to both of my parents, who have sacrificed much so that I could pursue my dreams of higher education. They provided the necessary support which gave me every opportunity to succeed.

Lastly I would like to thank the six months long, dreary, sunless, lifeless, cold, damp winters that central Illinois provided throughout my 5 years in graduate school, without which, I might have had too much fun…

TABLE OF CONTENTS

CHAPTER 1

INTRODUCTION

Geoelectric fields can be induced at the earth's surface during geomagnetic storms and high-altitude electromagnetic pulses (HEMPs). These fields drive damaging dc currents, geomagnetically induced currents (GICs), into the electricity grid through Y-grounded transformers. GICs have caused widespread power outages (1989, Quebec) and they have damaged large electrical equipment, such as high voltage transformers [1]. The North American Electric Reliability Corporation (NERC) identifies the two primary risks associated with geomagnetic disturbances (GMDs) as (1) damage to bulk power system assets, such as high voltage power transformers, and (2) voltage instability leading to a system collapse due to the loss of reactive power support [1] caused by transformer saturation and/or misoperation of protection devices leading to tripping of capacitors, etc.

HEMPs produce a low frequency burst of energy which interacts with the earth's magnetic field similar to the way a GMD interacts with the field, but more severely [2]. A HEMP is typically associated with a nuclear detonation in the atmosphere, at least 30 km above the surface of the earth. Detailed theory on the electromagnetic pulse generated by a HEMP can be found in [3]. The United States

and Russia performed independent testing of HEMPs in the 1960s. Due to the negative effects to the environment and to existing technology, the Nuclear Test Ban Treaty was passed in 1963 which banned nuclear weapon tests in the atmosphere, outer space, and under water [4]. The study of HEMPs has evolved into non-nuclear laboratory testing. These tests are usually much smaller than that of a HEMP, so the results are scaled accordingly. Another way to study HEMPs is through simulation. Simulation is beneficial when considering the effects on large, critical infrastructures, like the power grid. This chapter presents an overview of the HEMP phenomenon and its effects on the power grid.

The energy released from a HEMP manifests itself into three different electric field waveforms referred to as E1, E2, and E3, as seen in Fig. 1.

Figure 1 represents a standard design waveform developed by the International Electrotechnical Commission (IEC) to serve as a guideline for unclassified HEMP studies. Each of these electric fields affects power system assets differently, since their frequencies differ significantly from one another. Often, the modeling and simulation of different power systems phenomena are studied separately based on their time range of response. For example, it is not necessary to include boiler and other long-term dynamics when studying lightning propagation. The lightning disturbance will be over before the long-term dynamics have time to respond.

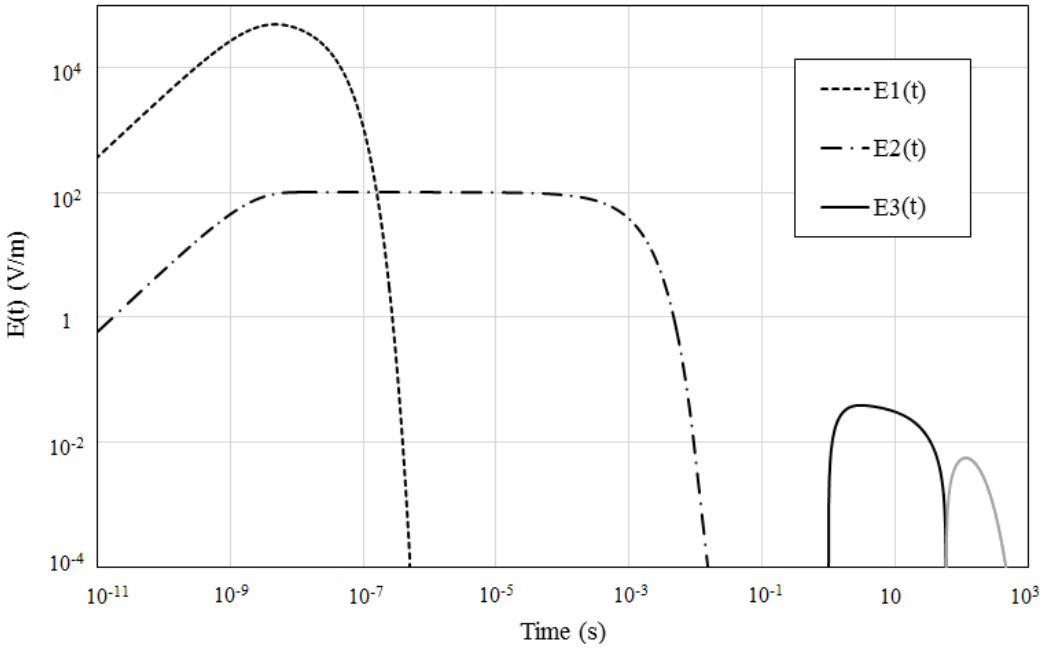

Fig. 1. Three electric field waveforms generated by a benchmark HEMP from IEC 61000-2-9 [5]

The two responses can be decoupled, from a time response perspective. Similarly, certain aspects of E1, E2, and E3 waveforms and their effects on the power system can be studied separately.

In 2003, an EMP commission was organized by the United States Congress to assess the following:

1. the nature and magnitude of potential high-altitude EMP threats to the United States from all potentially hostile states or non-state actors that have or could acquire nuclear weapons and ballistic missiles enabling them to perform a high-altitude EMP attack against the United States within the next 15 years;

2. the vulnerability of the United States military and especially civilian systems to an EMP attack, giving special attention to vulnerability of the civilian infrastructure as a matter of emergency preparedness;
3. the capability of the United States to repair and recover from damage inflicted on the United States military and civilian systems by an EMP attack; and
4. the feasibility and cost of hardening select military and civilian systems against EMP attack.

A description of their findings and recommendations is available in an executive report [6] and a critical national infrastructures report [7].

The vulnerability of critical national infrastructure is the primary driver for HEMP studies. Out of the infrastructures labeled critical, the electric power grid is considered the most critical by the EMP commission [7]. This is because almost all other infrastructures depend on the electric grid; transportation, emergency services, government services, oil and gas, communications and water, to name a few, require power to function adequately. Without electric power, all of the listed infrastructures will eventually fail.

The grid is not designed to tolerate catastrophic events that result in simultaneous impacts such as a HEMP. The HEMP three waves could leave the grid in a crippled state, full of damaged assets. Black start procedures and hardware do not exist to bring the grid back from such a devastated state. High voltage

transformers have a lead time on the scale of years, delaying the restoration of power to the affected regions. Furthermore, other critical infrastructures which would be used to restart the grid may have suffered damage as well; this includes transportation of fuel for the generators and communication systems as immediate significant examples.

Given the waveforms in Fig. 1 as a baseline, several power system components could be affected by a HEMP. The high frequency energy in the E1 waveform has the potential to couple into all unshielded electronic devices. E1 has a rise time of a few nanoseconds. The higher the electric field, the more potential there is for damage in electronic devices. From a power system perspective, this energy can couple into protective relays, SCADA system components, digital control systems (DCSs), programmable logic chips (PLCs), and communication systems. The EMP commission exposed these systems to simulated EMP, by performing free field testing as well as current injection testing. Failures in all tested devices were noted. The damage was quantified to increase 10 fold with every doubling of the electric field. The failures came in a number of forms, ranging from physical damage to the corruption of data.

Due to the extremely high electric field of E1, arc flashovers occurred on small electronic devices. SCADA provides data acquisition and control to the power system over large geographical areas. SCADA systems under the envelope of the EMP will all simultaneously be receiving/sending corrupted data and actions

to the grid under the duress of an EMP. The control system does not know that the data has been corrupted and will send improper control signals to the protective relays and other devices which control the power grid. This can lead to improper load shedding, resulting in the collapse of the power system as the frequency deviates beyond its defined operating region. In the distribution system, arcing across insulators and pole mounted transformers is of high concern. This translates to a loss of load, causing the frequency to uncontrollably increase beyond its limit, thus making the power system unstable.

High valued assets in the power system, such as high voltage transformers, are protected by relays and switching mechanisms. If significant damage from E1 occurs, the high valued assets will be left exposed and vulnerable to the oncoming E2 and E3 waves of the blast. The E2 wave is similar to a lightning strike, except it is widespread and happens simultaneously throughout the grid. Even though the magnitude of E2 is less than a lightning strike, the existing protection in the electric grid is not designed for such a widespread simultaneous impact. The higher frequency energy of the E1 and E2 waves have the potential to couple into long unshielded conductors, effectively becoming radiative antennas. The impacts of E1 and E2 waves on power systems were studied with electromagnetic transient pulse tools in [8], [9].

E3 waves induce violent fluctuations in the earth's magnetic field. These currents are large enough to damage high value transmission system components,

like generator step-up transformers. The transformer cores become saturated by means of the dc current. As a result, the transformers suffer hot spot heating, produce even and odd harmonics, and consume reactive power. The E3 wave itself can further be divided into two waves, E3A and E3B. The E3A wave is a result of the magnetic field distortions due to the initial nuclear blast. The E3B wave is the result of a later, slower magnetic field distortion due to the weapon's energized debris. The research on the effects of E3 on the electric grid is usually associated with steady-state, solar storm induced GMD analysis. While E3B and GMDs share similar magnitudes and rise-times, E3A has higher magnitudes and rises much faster. Similar to E3, solar storms cause variations in the earth's magnetic field, which induce geoelectric fields and thus GICs.

Existing HEMP E3 studies on the power grid have been performed using GMD power flow analysis [10]. As previously mentioned, this analysis is inadequate for HEMP E3 due to the quick rise times associated with the disturbance. In [10], a background of HEMP E3 is given, as well as its potential impacts to the bulk United States electric grid, through a series of studies. Each study assumes a different blast scenario and discusses which systems would be affected. In each scenario, potential damage to circuit breakers, EHV transformers and GSU transformers are cited. However, like most research, the document avoids concluding that a disturbance like this will collapse the grid. Instead the document states that such a result is possible.

Historically, GICs due to GMDs have caused long-lasting blackouts and damage to power system hardware [11]. Lumping E3 and GMD research together provides a general understanding of how E3 can affect the grid. It is convenient that the two topics share this commonality, but it is important to recognize and study their differences.

CHAPTER 2

INCORPORATING GIC MODELING INTO TRANSIENT STABILITY

GIC enters and leaves the grid through wye-grounded transformers, Fig. 2.

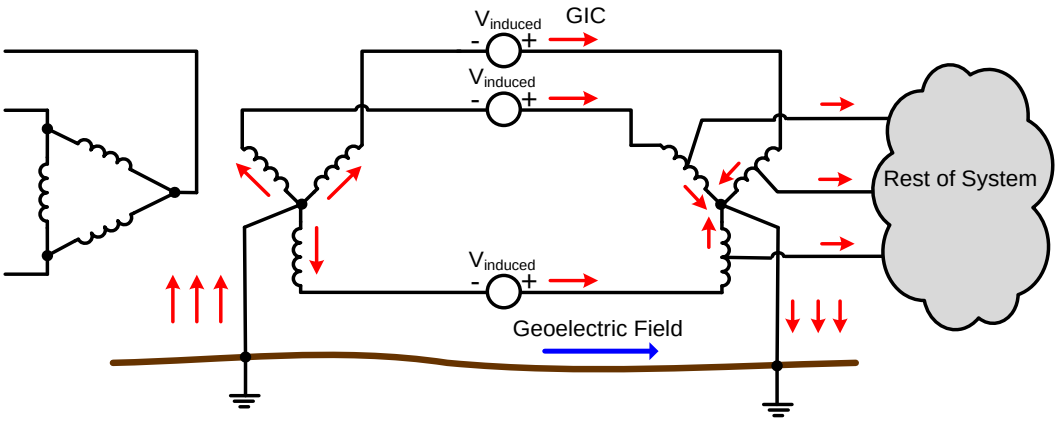

Fig. 2. Illustration of GIC flow in a power system [12]

Early information on the inclusion of GIC in the power flow can be found in [13] and later, with the consideration of large systems, in [14], [15]. Originally, the electric field variation was represented as dc voltage sources in the ground, in series with the substation grounding resistance [13]. While this method is valid for uniform geoelectric fields, it was later shown that for non-uniform geoelectric fields it is more accurate to model the dc voltage sources in the transmission lines

themselves [16]. The geoelectric field induced line voltages, $V_{induced}$, are calculated according to

$$V_{induced} = \oint_{\Sigma} \bar{E} \cdot d\bar{l} \ , \tag{1}$$

where $\bar{E}$ is the geoelectric field and $d\bar{l}$ is the incremental distance along the transmission line path, Σ. Next, the field induced line voltages are represented as Norton equivalent current injections, **I**, and used to calculate the dc bus voltages of the system, **V**, according to

$$\mathbf{I} = \mathbf{GV} \ . \tag{2}$$

G is a square matrix comprised of the power network's conductance values. The elements of **G** are determined by the parallel combination of the lines' three phases. It has similar form to the system admittance matrix except the values are purely real and the matrix is augmented to include substation neutral buses and substation ground resistance values. With the system's dc bus voltages known, the GIC, in its respective branch, can be calculated using Ohm's law.

To demonstrate the calculation of GIC flow in detail, consider the four bus power system in Fig. 3. The system has been exposed to a left-right geoelectric field of 1.5 V/km. The length of the transmission line between buses 1 and 3 is 100 km.

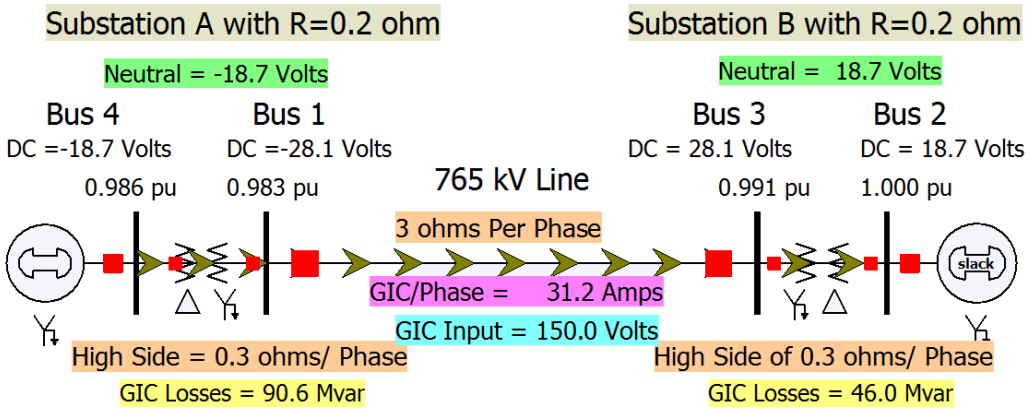

Fig. 3. One-line diagram of four bus system

This system has two generators, two high voltage generator step-up transformers that are grounded wye, and a high voltage transmission line connecting the two transformers. The integration of the electric field has already been performed and an induced dc voltage source value of 150.0 V results. The 150 V serves as an input to this GIC model. The brown arrows represent the direction and magnitude of the calculated GIC. Explicitly noted in the one-line diagram are the substation grounding resistances, transformer winding resistances, and the resistance of the transmission line. All of these values are required to accurately calculate the GIC. The GIC is calculated by first augmenting the system to include the substation ground buses and then performing nodal analysis. The dc circuit is shown in Fig. 4.

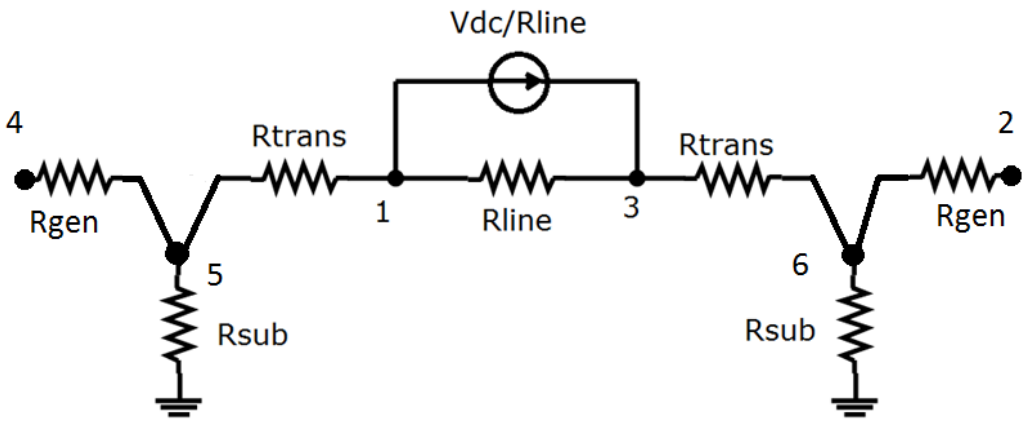

Fig. 4. Augmented dc network

The first thing to notice is that the diagram now includes buses 5 and 6, with open ends on nodes 2 and 4. The existence of the delta connection between buses 1 and 4, and buses 2 and 3 prevents the GIC from flowing through generators. The inline voltage source has been converted to its Norton equivalent, and will serve as a current injection in the nodal analysis. Also, consistency in single phase, or three phase value of resistance is of high importance. The GIC enters and exits through the grounded transformers but it splits evenly among the three phases of the transmission line. In the following calculations, three phase resistance values are used. Symbolically, (2) evaluates to

$$\begin{bmatrix} -V_{dc}/R_{line} \\ 0 \\ V_{dc}/R_{line} \\ 0 \\ 0 \\ 0 \end{bmatrix} = \begin{bmatrix} G_{11} & 0 & G_{13} & 0 & G_{15} & 0 \\ 0 & G_{22} & 0 & 0 & 0 & G_{26} \\ G_{31} & 0 & G_{33} & 0 & 0 & G_{36} \\ 0 & 0 & 0 & G_{44} & G_{45} & 0 \\ G_{51} & 0 & 0 & G_{54} & G_{55} & 0 \\ 0 & G_{62} & G_{63} & 0 & 0 & G_{66} \end{bmatrix} \begin{bmatrix} V_1 \\ V_2 \\ V_3 \\ V_4 \\ V_5 \\ V_6 \end{bmatrix}. \qquad (3)$$

Since the resistance of the generators is not known, a value of 1 is assigned, to prevent the conductance matrix from being singular. It should be clear that this number only assists in the matrix inversion. Since there is no current flow in the branch connecting nodes 4 and 5, the assigned resistance does not matter, as long as the chosen value does not make the matrix ill conditioned. Substituting the values into (3) and solving, the following dc voltages result,

$$\begin{bmatrix} 11 & 0 & -1 & 0 & -10 & 0 \\ 0 & 1 & 0 & 0 & 0 & -1 \\ -1 & 0 & 11 & 0 & 0 & -10 \\ 0 & 0 & 0 & 1 & -1 & 0 \\ -10 & 0 & 0 & -1 & 16 & 0 \\ 0 & -1 & -10 & 0 & 0 & 16 \end{bmatrix}^{-1} \begin{bmatrix} -150 \\ 0 \\ -150 \\ 0 \\ 0 \\ 0 \end{bmatrix} = \begin{bmatrix} V_1 \\ V_2 \\ V_3 \\ V_4 \\ V_5 \\ V_6 \end{bmatrix} = \begin{bmatrix} -28.125 \\ 18.75 \\ 28.125 \\ -18.75 \\ -18.75 \\ 18.75 \end{bmatrix} \text{ V.} \quad (4)$$

The three phase GIC flow can now be calculated by Ohm's law, in accordance with the system topology,

$$\text{GIC}_{3\phi} = G_{\text{sub}} V_5 = (5)(-18.75) = -93.75 \text{ A.} \quad (5)$$

The GIC in each phase of the transmission line can be found by dividing the three phase GIC by three, to achieve 31.25 A [17]. For large systems, sparse vector methods are employed for the calculation of **V**.

GIC can cause half-cycle saturation in high voltage power transformers. This saturation translates into increased reactive power losses in the transformer, among other things. The exact relationship between the GIC and the reactive power losses is an ongoing research effort. Based on [18], [19], [20], the transformer's

reactive power losses vary linearly with the terminal voltage. In per unit form, a reactive power loss relationship with respect to the GIC could be written as

$$Q_{Loss,pu} = V_{pu} K I_{GIC,pu} \ , \tag{6}$$

where V_{pu} is the transformer terminal voltage in per unit, K is a transformer type dependent scaling factor which is unitless, I_{GIC} is an "effective" GIC in pu which is also transformer type dependent, and Q_{Loss} is the reactive power loss in pu of the transformer. The need for a transformer type dependent scalar, K, and effective GIC, I_{GIC}, arises from the fact that different transformer configurations and transformer types facilitate neutral current flow and core saturation differently, Fig. 5. For example, in an autotransformer, the GIC actually flows through the transformer, since it is not electrically isolated like a generator step-up transformer would be.

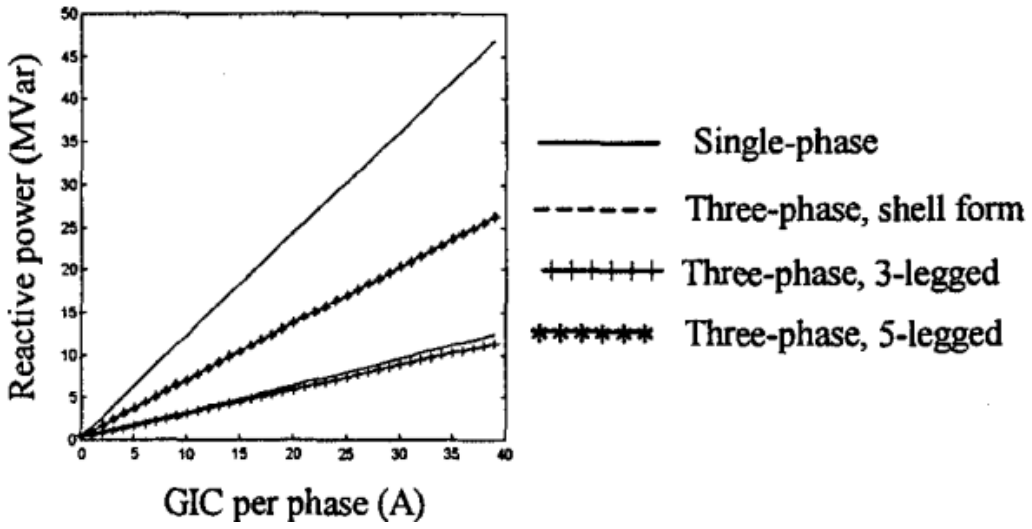

Fig. 5. The variation of the MVar consumption vs. the input GIC per phase [18]

The *K* value is derived from the slope of the lines in Fig. 5. More work on how GICs flow through transformers and mapping the transformer losses due to GIC into the power flow is shown in [15]. Experimental work with GIC in transformers was performed in [21], also showing a linear mapping between the reactive power losses and GIC.

Some of the lingering questions of model verification and validation in this research area are beginning to be addressed. More monitoring equipment is being installed. As a result, more data is being made available for researchers. However, there are still gaps in some of the modeling of the system components. Ideally, all the model parameters, such as substation grounding resistance, transformer winding resistance, transformer configuration, to name a few, would be known. These parameters are usually known only by the owners of the equipment, i.e. the utility. If the real data for these parameters is unknown to the model, the values must be estimated in order to calculate the GIC. The impact these estimations have on the system are beginning to be studied. The sensitivity of GIC to substation grounding resistance is introduced in [22], with the conclusion being GIC can be quite dependent on the substation grounding resistant values.

Another area of model uncertainty is the problem of how to model the delay between GIC flow and saturation. This delay is very important because it determines when the transformers begin to consume reactive power due to GIC saturation. Little research has been done in this area, however, results point toward

a delay on the order of a few seconds [23], [24]. This dissertation first contains simulations based on a zero time delay between the GICs and the onset of transformer saturation. Later, the simulations use a first-order lag delay. The delay length tends to be transformer specific. So, a simple general model was created which delays the saturation by a user-selected number of seconds.

When performing power system GIC studies, it is important to understand the impacts of neighboring systems. For example, is it necessary to calculate the impacts of GIC throughout the entire Eastern Interconnect to determine the impacts to a specific utility? An algorithm for determining system sensitivity GIC line flow is presented in [25], indicating that systems outside the surrounding area of interest play little role.

Special attention should be given to the quick rise-times and large magnitudes of electric fields induced by HEMPs; in particular, how HEMPs fit into the dynamics of the electric grid. Figure 6 depicts how the HEMP waveforms align with the time responses of power system dynamics.

Comparing this with Fig. 1, it is clear that all frequencies emitted by a HEMP interact with the power system to some extent. Figure 6 also directs researchers toward the appropriate modeling and simulation detail needed when considering HEMPs and their effects on the power system. The time response of transient stability, along with governor and load frequency control, align directly with E3.

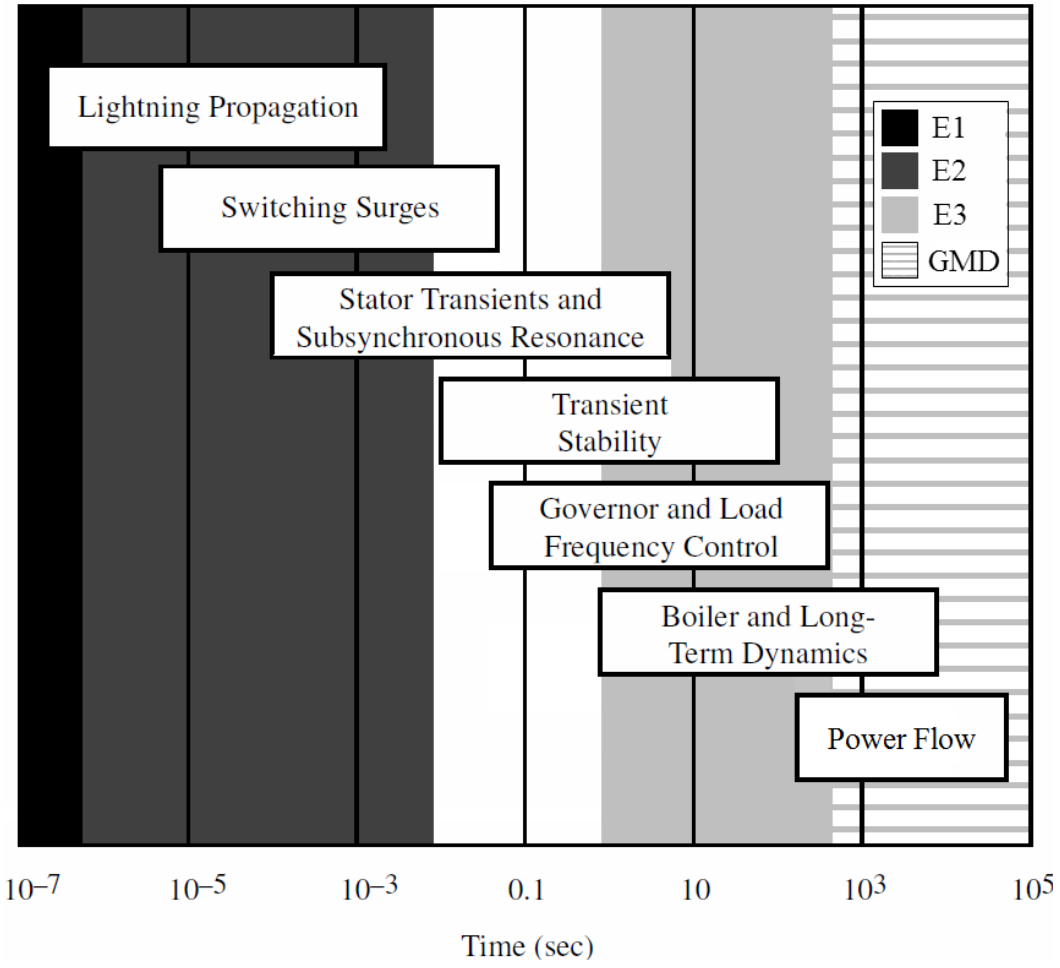

Fig. 6. Potential impacts of a HEMP to a power system correlated by their time range response, adapted from [26]

Geomagnetic storms are usually not studied in the transient stability time frame. Their typical rise-times of minutes makes them appropriate for power flow studies. This is not to say that a storm could not produce rise-times that would fall into the transient stability domain. Rise-times of GICs on the order of 30 seconds have been recorded [27]. Preliminary consideration of voltage stability impacts of

GMD induced GIC has recently been studied [28]. The authors showed that GMD-type disturbances with quicker rise-times warrant transient stability analysis.

HEMP E3 has rise-times on the order of seconds, where GMDs have rise-times on the order of minutes. HEMP E3 is a prime candidate for large disturbance, short-term transient stability analysis, thus motivating this research.

E3 induces violent fluctuations in the earth's magnetic field due to magneto-hydrodynamic effects. The changes are so violent that GICs on the order of hundreds to thousands could propagate in the grid [7]. These currents are large enough to damage high value transmission system components, like generator step-up transformers. The transformer cores become saturated by means of the dc current. As a result, the transformers suffer hot spot heating, produce even and odd harmonics, and consume reactive power.

The E3 wave itself can further be divided into two waves, E3A and E3B. Examination of test data from before the nuclear test ban treaty was in effect, as well as advances in theoretical and numerical modeling, lead to the qualitative understanding of the E3A and E3B fields available now.

E3A is a result of the geomagnetic field distortions due to the initial nuclear blast. A magnetic bubble is formed due to the geomagnetic fields being pushed ahead of the conducting region. The expansion of the bubble is a function of the speed of the weapon debris, density of the atmosphere, and altitude. Seen from a distance, the perturbation of the field resembles a dipole, aligned with the

geomagnetic field lines at the blast location. The time of day, as well as the solar cycle, can affect the strength and timing of the induced fields. A detonation during times of heightened solar activity will tend to slow down the expansion and collapse of the magnetic bubble, thus decreasing the induced field magnitude.

Figure 7 is an image of the earth overlaid with a contour of the peak field magnitudes for E3A. The areas describe the electric field direction. This scenario assumes the EMP was detonated over central Mexico, 400 km above the earth.

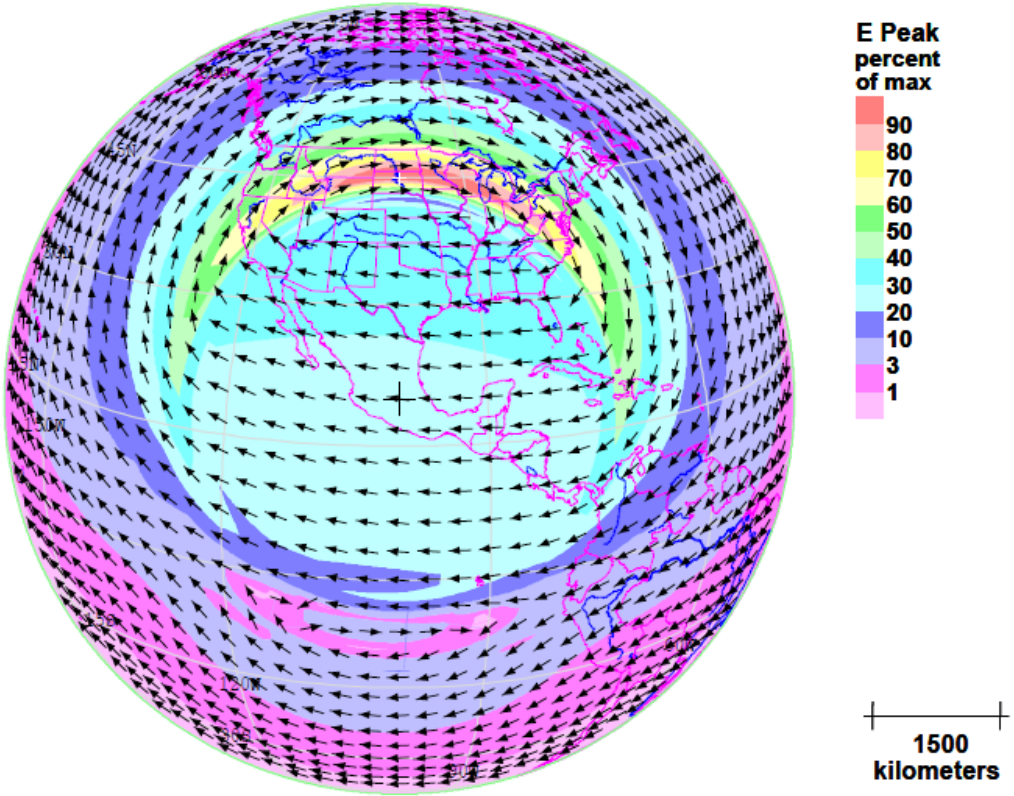

Fig. 7. Spatial variation of E3A for a detonation 400 km above central Mexico [10]

The most intense areas of the field occur over the northern United States. It can be seen that a very small amount of the earth, or even the United States, experiences fields higher than 35-40% peak. For this dissertation, spatial distribution data from [10] will be combined with the temporal/magnitude evolution data from [5] in order to use more realistic electric field scenarios in simulations.

The ground is shielded directly under the blast. This is due to the first emitted x-rays intensely ionizing a patch in the atmosphere, directly beneath the blast. This highly conductive patch protects the underlying area from the vertical penetration of the magnetic fields. As a result, the fields experience a sliding effect and the most intense fields are seen at the edge of the patch, oriented perpendicularly to the magnetic fields [10].

E3B is the result of a later, slower magnetic field distortion due to the weapon's energized debris, inside the magnetic bubble, following the geomagnetic field lines. The debris heats up, ionizing the upper atmosphere, causing it to buoyantly rise and expand. The center of the ionized region is heated more, causing it to rise faster than the edges. This rising plasma passes through geomagnetic field lines, inducing currents due to the dynamo effect. Currents begin to flow in the ionized region, in turn, inducing magnetic fields at the surface of the earth. Figure 8 shows the spatial variation of the E3B geoelectric field for a blast above the central continental United States, 130 km in altitude [10]. A quantitative electric

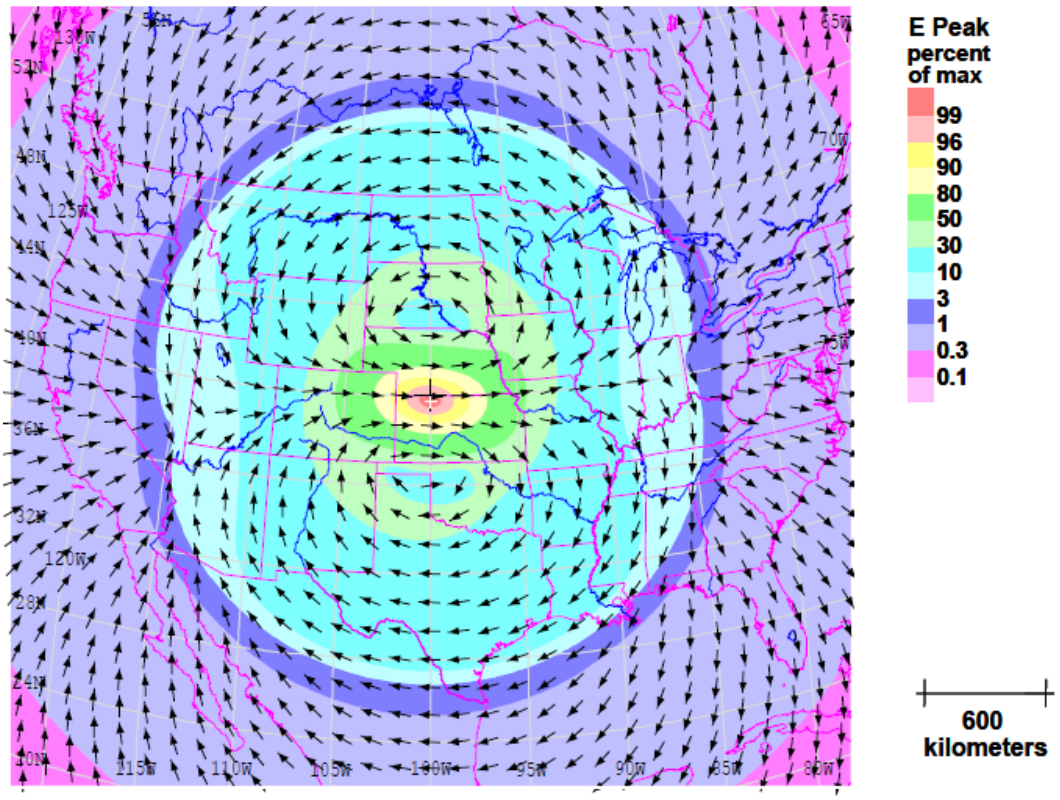

Fig. 8. Spatial variation of E3B for a detonation 130 km above central continental United States [10]

field waveform for E3B is provided by [10]. The authors of [10] admit, “many aspects of the model should not be taken too seriously”, (pp. 2-11). They believe the electric field falls more rapidly than the model they provided.

The IEC provides equations for unclassified use, which describe the induced geoelectric field for E1, E2, and E3 [5]. A composite E3 wave is given by,

$$E_3(t) = E_i(t) - E_j(t)\ , \tag{7}$$

$$E_i(t) = \begin{cases} 0 & \text{when } \tau \le 0 \\ E_{0i} \cdot k_i \left(e^{-a_i \tau} - e^{-b_i \tau} \right) & \text{when } \tau > 0 \end{cases} \tag{8}$$

$$\begin{aligned} &\tau = t - 1 \\ &E_{0i} = 0.04 \text{ V/m} \\ &\mathrm{a}_i = 0.02 \text{ s}^{-1} \quad , \\ &b_i = 2 \text{ s}^{-1} \\ &k_i = 1.058 \end{aligned}$$

and

$$E_j(t) = \begin{cases} 0 & \text{when } \tau \le 0 \\ E_{0j} \cdot k_j \left(e^{-a_j \tau} - e^{-b_j \tau} \right) & \text{when } \tau > 0 \end{cases} \tag{9}$$

$$\begin{aligned} &\tau = t - 1 \\ &E_{0j} = 0.01326 \text{ V/m} \\ &\mathrm{a}_j = 0.015 \text{ s}^{-1} \quad . \\ &b_j = 0.02 \text{ s}^{-1} \\ &k_j = 9.481 \end{aligned}$$

The curve in Fig. 9 is described by (7), (8), and (9). The waveform is considered composite because it combines E3A and E3B. The waveform assumes a uniform ground conductivity of $\sigma_g = 10^{-4}$ S/m. For other ground conductivities, the electric field scales according to E3$\sim {\sigma_g}^{-1/2}$. No guidance is given in regard to the spatial variation of the geoelectric field in [5]. The composite wave is discretized

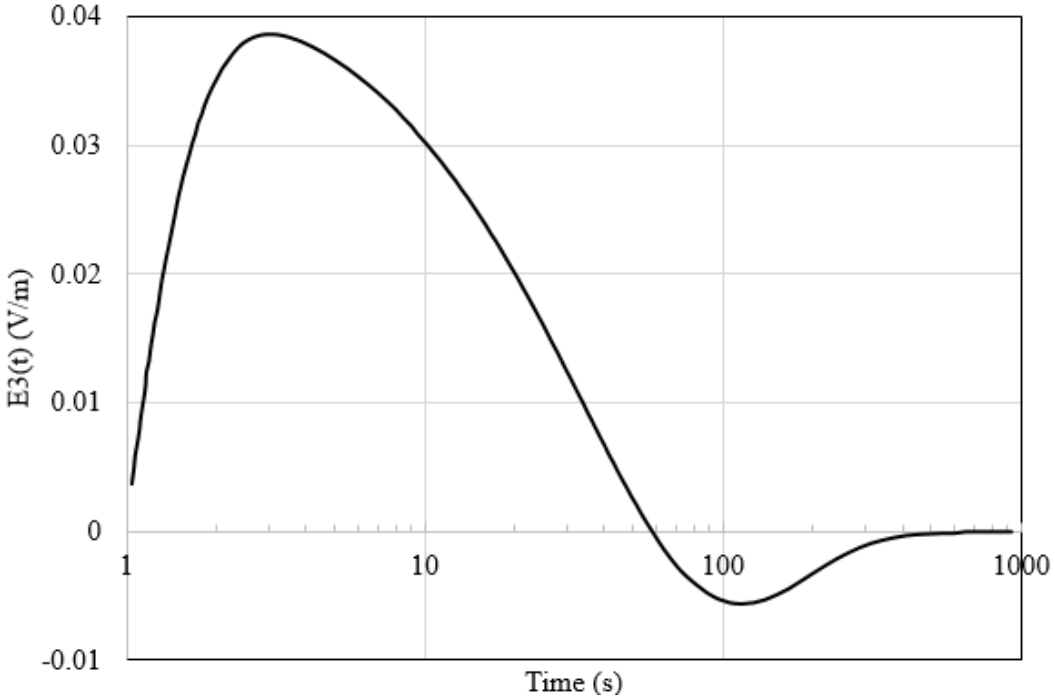

Fig. 9. $E_3(t)$ waveform in V/m

into 140 samples, Fig. 9, to serve as input electric field data to the simulations in this dissertation.

A concern that must be addressed is determination of what strength of electric fields should be applied to which regions for E3A. In order to simulate the HEMP on a power network, certain detonation parameters must be assumed. The IEC waveform is a time-varying uniform field, lacking spatial variation. A uniform field simulation is a good start; however, a more realistic approach would be to analyze the impacts of different peak field magnitudes according to possible field distributions. One possible field distribution is shown in Fig. 7.

The later, E3B, wave begins at approximately 60 seconds. Since the fields vary so slowly, minutes to hours, the dynamics no longer play an important role in the modeling. Hence, E3A and E3B can be decoupled and studied separately. Steady-state GMD analysis methods can be applied to E3B. Dynamic, transient stability analysis is needed for studying E3A. The focus of this dissertation is dynamic analysis of E3A.

The transient stability problem consists of integrating differential algebraic equations of the form,

$$\dot{x} = f\left(\underline{x}, \underline{y}\right) \tag{10}$$

$$0 = g\left(\underline{x}, \underline{y}\right), \tag{11}$$

where (10) are differential equations representing the dynamics of the system, and (11) are the stator algebraic and network equations. The *x* represents the dynamic state variables, and *y* represents the power flow state variables such as bus voltage and angle. The equations are determined by the types and parameters of dynamic models used in the simulation, as well as the characteristics of the underlying power system network.

The additional reactive power loading due to the GIC saturated transformers can be modeled in the network algebraic equations. The reactive power losses due to GIC are represented as a constant reactive current load since the losses vary linearly with voltage while the current remains independent. Since a load can be

present at a generator bus or a load bus, the reactive power balance equations are shown for each in (12) and (13), respectively.

$$Q_{Gen,i} + Q_{L,i} + Q_{Loss,i} - \sum_{k=1}^{n} V_i V_k Y_{ik} \sin\left(\theta_i - \theta_k - \alpha_{ik}\right) = 0, i = 1, ..., m \qquad (12)$$

$$Q_{L,i} + Q_{Loss,i} - \sum_{k=1}^{n} V_i V_k Y_{ik} \sin\left(\theta_i - \theta_k - \alpha_{ik}\right) = 0, i = m+1, ..., n \qquad (13)$$

$Q_{L,i}$, from (12) and (13), is the sum of the reactive load at bus i and the reactive power loss due to GIC at bus i, from (6). $Q_{Gen,i}$ is the reactive power supplied by the generator at bus i. V_i is the voltage at bus i. Y_{ik} and α_{ik} are the admittance and admittance angle, respectively, between buses i and k. The bus angle is given by θ. There are m generator buses and n total buses. The real power network equations are not shown here, since the loading on the transformers due to GIC is strictly reactive. The impact of existing transformer loading is not accounted for in this model. In a real power system, transformers already operating near their maximum VA rating will enter saturation faster during a GMD than similar transformers that are not as heavily loaded, and hence would demand reactive power sooner. In this research, neither existing non-GIC loading nor proximity to saturation is considered in the calculation of Q_{Loss}. The reactive power losses due to GIC are represented as a constant reactive current load since the losses vary linearly with voltage.

CHAPTER 3

DYNAMIC MODELING IMPACTS

There is a variety of static and dynamic models for electric machines, exciters, governors, stabilizers, and loads. Different models are appropriate for different studies. For example, the GENROU model provides a good approximation for the behavior of a synchronous generator over the dynamics of interest during a transient stability study. A variety of models used in WECC studies can be found in [29].

As mentioned in Chapter 2, the E3 impacts can be modeled as a large-disturbance, short-term voltage stability problem. Hence, the load models used in the system will play a major role. Load modeling is a challenging aspect of dynamic system modeling. Depending on the response time of the disturbance, among other things, load models can significantly impact transient stability results. The load is constantly changing, with key diurnal and temperature variations. The model should hold valid for low voltages due to disturbances that may occur in transient stability.

Load models can be generally categorized into two types, static and dynamic. Static load models use algebraic functions of the bus voltage, and

sometimes the frequency. Constant impedance, current, and power load models are examples of static models. Dynamic load models can incorporate motor dynamics, which are usually dependent on the states of the power system. More on load modeling can be found in [30], [31]. Both model types are studied in this chapter.

The test case used for the studies in this chapter is derived from the 20 bus GIC benchmark test case from [32]. The test case consisted only of dc network information. Ac power flow data, as well as dynamic models and their parameters (see Appendix A) have been added in this chapter to this case to make it suitable for ac transient stability studies. The case features a 20 bus EHV network of 500 kV and 345 kV voltages. The single line diagram of the system is shown in Fig. 10.

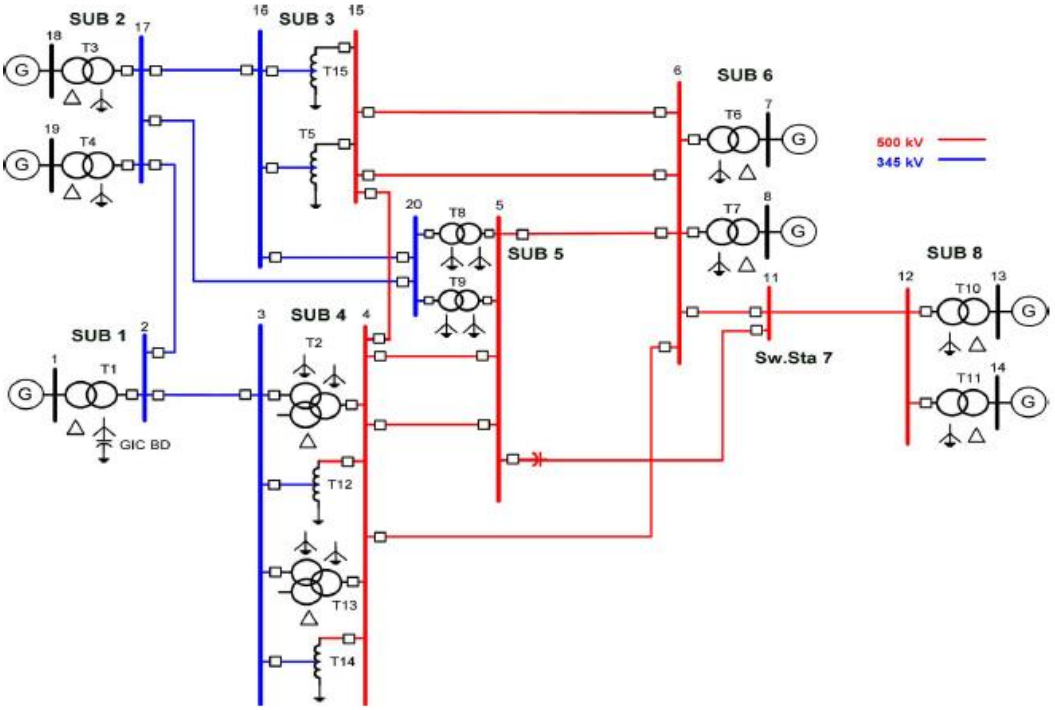

Fig. 10. The 20 bus test case for the calculation of GIC [32]

There are a variety of transformers, including auto-transforms, generator step-up transformers, as well as two and three winding transformers. The transformers are configured in a number of ways depending on their windings. Delta wound transformers are modeled in the test case, even though they do not allow GIC to flow through them. It should be noted that there are two GIC blocking devices in this test case. One of the blocking devices is a capacitor placed in the neutral grounding connection of T1, located in substation 1. The second is a series capacitor placed between buses 5 and 11. Both these devices prevent GIC flow through their respective branches.

In order to make the case suitable for ac power flow and dynamic stability studies, typical 500 kV three conductor bundling and 345 kV two conductor bundling ac line parameters were added.

The transient stability studies in this chapter use an integration time step of ¼ cycle. The large disturbance being applied to the system is the increased reactive loading at transformer buses, arising from the GICs caused by the E3A electric field, approximately the first 60 seconds of the composite HEMP E3 wave from [5].

The initial power system operating point is kept constant for all the studies. In a real power system, transformers already operating near their maximum VA rating will enter saturation faster during an EMP than similar transformers that are not as heavily loaded, and hence would demand reactive power sooner. In this

dissertation, neither existing non-GIC loading nor proximity to saturation is considered in the calculation of Q_{Loss}.

It is important to note that protection systems and models such as generator over-excitation limiters or under-voltage relays have not been modeled in the test system for simplicity, since the focus of the studies that follow is to provide example analyses of load models responding to an E3A disturbance. Basic protection system inclusion is considered later in the chapter.

Static load models are commonly used in transient stability studies. Often, the frequency dependence of the load is neglected, resulting in the ZIP model. The ZIP model is implemented using (14).

$$\begin{aligned} P_L &= P_0\left[\, p_1\bar{V}^2 + p_2\bar{V} + p_3 \,\right] \\ Q_L &= Q_0\left[\, q_1\bar{V}^2 + q_2\bar{V} + q_3 \,\right] \end{aligned} \tag{14}$$

P_L and Q_L are the active and reactive components of the load. $\bar{V}$ is a vector of the bus voltages. The model is composed of constant impedance (Z), constant current (I), and constant power (P) components. The coefficients p_1 to p_3 and q_1 to q_3 are the proportions of the load components, respectively. These parameters can be adjusted so that they accurately model the load, constrained such that the coefficients sum to one for each equation.

The power system shown in Fig. 10 is subjected to the first 60 seconds of the HEMP induced electric field waveform of [5] for a static load model configuration. The load was modeled as 100% constant impedance. Four

simulations were run with this load configuration. Each simulation assumed peak geoelectric fields to be a fraction of the peak value in Fig. 9, namely 40%, 70%, and 100%, respectively. The fractions were chosen based on the spatial distribution of [10], assuming the system lies within a single region. A larger network could certainly span different peak value regions. For the 70% scenario, a series of steady-state solutions was compared to the transient stability results. Series of steady-state solutions are often used to study voltage collapse in GMD analysis, wherein the electric field is increased in gradual steps of 0.5 or 1 V/km followed by calculating the GICs and losses. Here, the transient stability results and steady-state results do not match, as seen in Fig. 11, even with a step size as small as 0.01 V/km. The disturbance is changing at a rate that alters the dynamic response of the system, something that is not apparent in the steady-state solution.

Shortly before the disturbance reaches its maximum, the steady-state solution experiences a blackout, misrepresenting the dynamic response of the system. The lowest bus voltage, bus 3, is shown over the length of the disturbance in Fig. 11. The shape of the E3 wave is also shown in Fig. 11 to show how the disturbance relates directly to the change in the voltages. For 40% scaling, the bus voltage dips just below 0.8 pu, for less than a second and below 0.9 pu for less than 10 seconds.

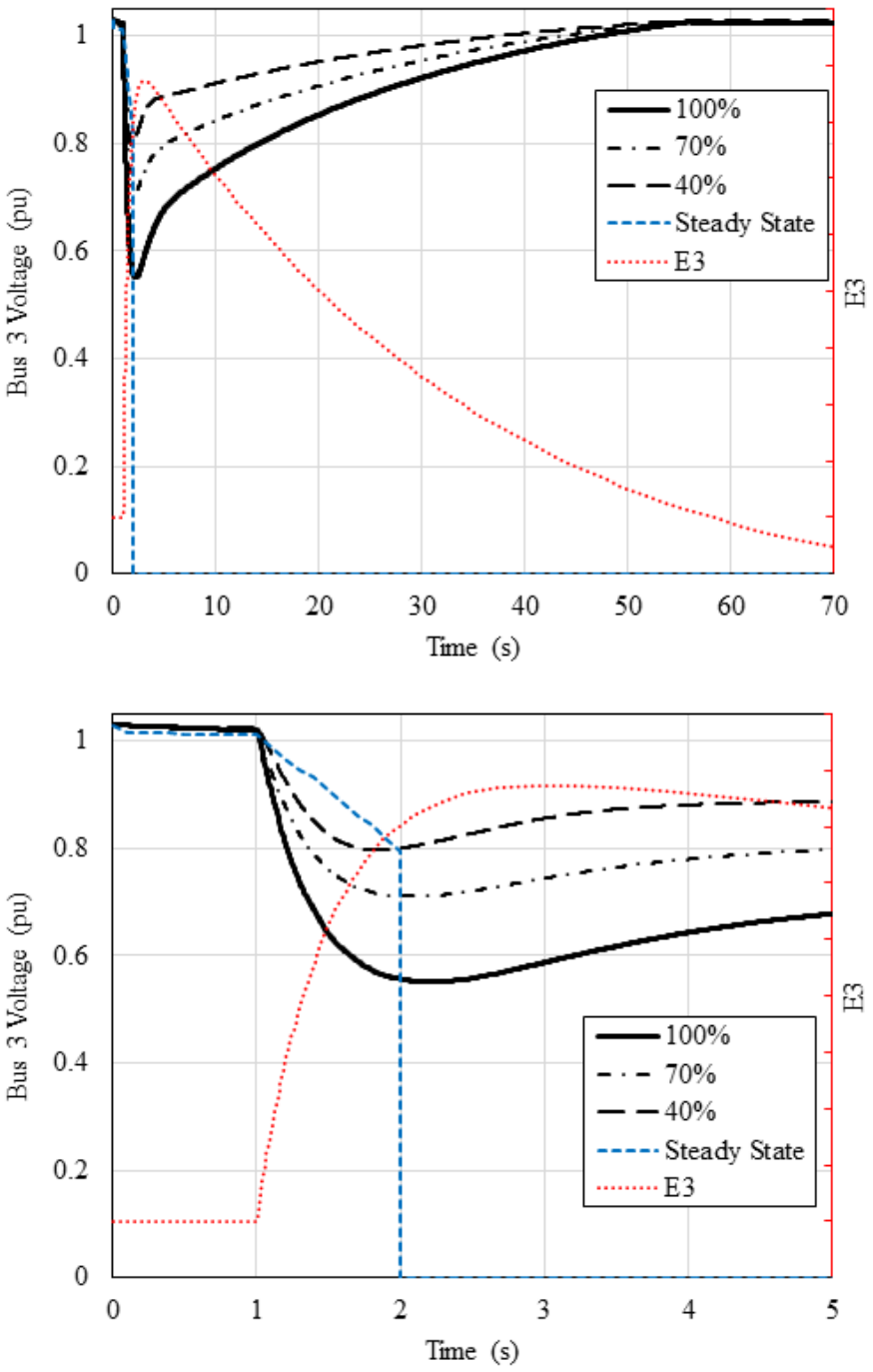

Fig. 11. Bus 3 voltage for 100% constant Z load with HEMP E3 overlay

According to the proposed distribution of Fig. 7, most of the network would be in the 40% or less peak field regions. These initial studies are more valuable qualitatively than quantitatively. Understanding how existing load models respond to the simulated disturbance will provide insight to future HEMP E3 impact studies.

As expected, the increased reactive power demand causes a rapid decline in the system bus voltages. It is important to note that the reactive power demand due to the disturbance, Q_{Loss} changes linearly with the terminal voltage of the transformer according to (6). The reactive power of the load, Q_L, is described by (14), with the constant Z load decreasing with the square of the bus voltage. Constant current and constant power load models will be more demanding than constant impedance load models under this E3 disturbance.

The transient stability study shows that for this particular system, the buses that suffered the largest voltage drops were those furthest from the generation. The buses that are impacted the least are those closest to the generation. These two observations are not surprising. The buses further from the generation also have loads attached to them and are closer to the saturated high voltage transformers, thus intensifying their voltage drops.

The transient stability analysis becomes more complicated when dynamic load models are considered. The models can include machine dynamics, often induction machines, to better characterize the load. Dynamic load models make such studies more realistic since a portion of the actual load is comprised of motors.

However, dynamic load model data is not always available, or known. It is often debated which models best represent the system response. There are several models to choose from when modeling a system's load. This chapter uses the MOTORW load model [29], which is a commonly used three-phase induction motor model that represents aggregates of individual motors. The MOTORW model also includes a basic undervoltage relay which controls the state of the dynamic portion of the load. The MOTORW parameters used are shown in Appendix B.

Another advantage of studying HEMP in transient stability is the ability to include the protection system. A general trend of transient stability studies is that they are increasingly including parts of the protection system. With proper protection systems in place, portions of the load would likely trip due to low voltage/damage. This leads to an important realization that protection systems could be configured in a way that could mitigate the effects of GIC. This key insight is recognized through studying the HEMP E3 problem in the transient stability domain, using dynamic models. This information is not apparent in steady-state simulations. Furthermore, less expensive mitigation strategies could be devised by configuring existing protection equipment accordingly.

The following three studies investigate dynamic load model response with and without the consideration of basic power system protection. The load is comprised of dynamic and static models. The dynamic model used is the MOTORW model. The static model is comprised of 75% constant impedance, 25%

constant power; this ratio was chosen as an example. The E3A intensity chosen for this study is 70%. The lowest bus voltage, bus 3, is shown for each study in Fig. 12.

Without the protection system, the induction motors head toward stall and a delayed voltage recovery ensues, as seen in Fig. 12. The stalling of the induction machines results in a large reactive power demand on the system. There is not enough generation to satisfy the demand of the saturated transformers and the system load.

Consider the same system and disturbance, but this time, basic undervoltage load relays are modeled into the induction motor portion of the load. If the relays are set to trip after being below 0.5 pu for 1 or more seconds, the systems voltage recovery is much quicker, as seen in Fig. 12.

In the event of a HEMP, it is likely that portions of the load will be damaged/tripped due to the E1 and E2 waves [7]. This unwarranted load shedding could actually prove to be beneficial to system stability/recovery while the system is under the duress of the following E3 wave. The combination of the saturated transformers with the existing system load results in an overloaded system. Consider the previous case of 100% load, showing the delayed voltage recovery. If 20% of the load is lost due to E1/E2 0.1 seconds before the E3 disturbance begins (1.1 seconds simulation time), the system experiences a much quicker voltage recovery, and suffers less of a penalty to the voltage magnitude, Fig. 12.

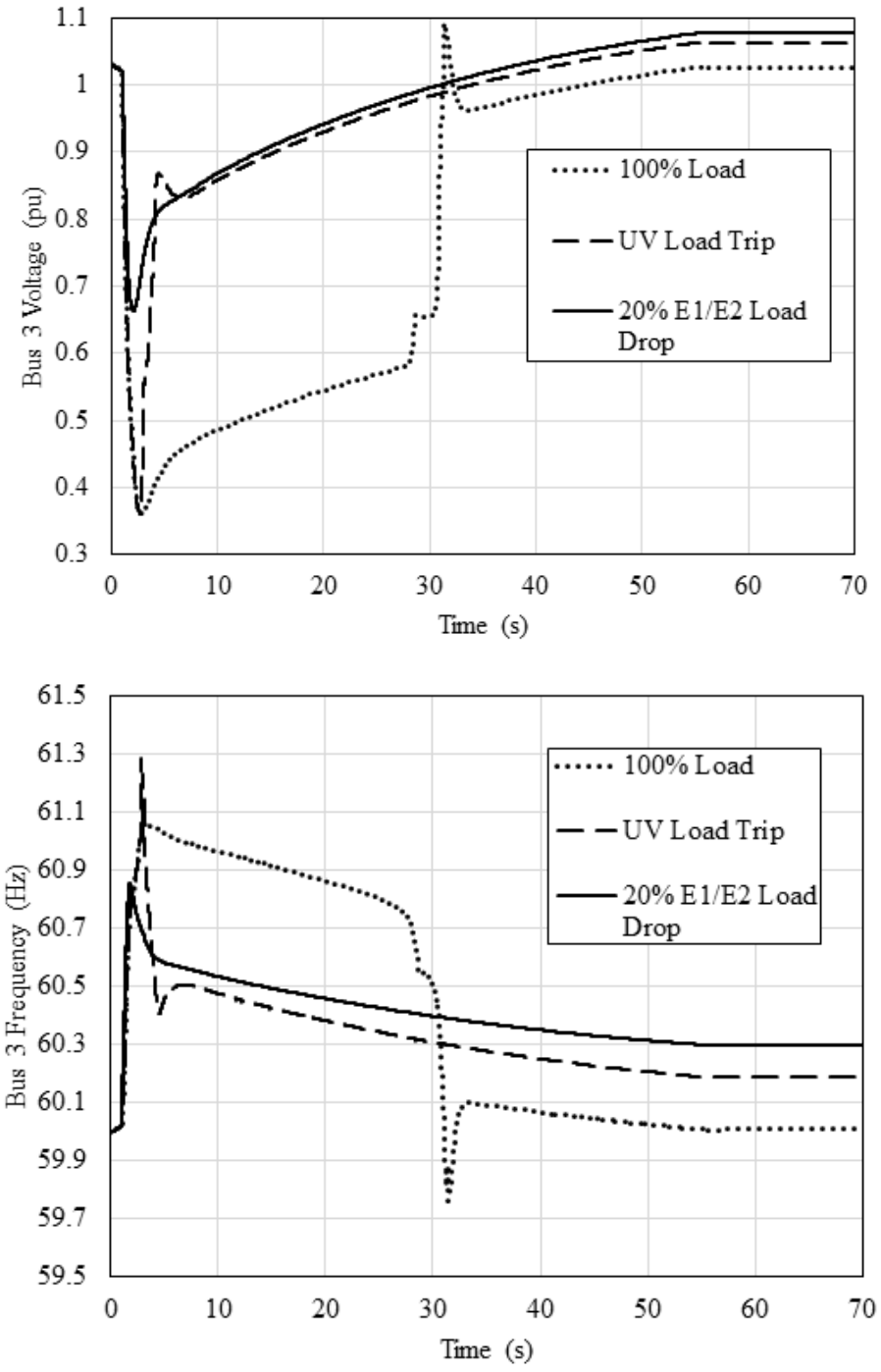

Fig. 12. Bus 3 voltage and frequency for dynamic load and mitigation scenarios

Suddenly losing large portions of the load can lead to frequency issues in the system. The frequency impacts are shown for each scenario in Fig. 12. Frequency constraints were not imposed during these simulations; however the frequency does not deviate more than 2.2% from the nominal value.

These are a few of many possible scenarios that show how dynamic power system components could respond during a HEMP. Many existing dynamic models are capable of responding to the HEMP E3 effects shown in this dissertation and are readily available in transient stability packages. By no means are these studies conclusive. These studies shed light on the importance of transient stability analysis of power systems during HEMPs.

This chapter has provided a methodology to model the impacts of HEMPs, specifically the E3A wave into power system transient stability simulations. It shows that the increased reactive power demand caused by the HEMP-induced GICs in transformers, in a time frame ranging in seconds, makes this a large-disturbance, short-term voltage stability problem. Since load models play a key role in such type of voltage stability assessments, example studies with static and dynamic load models were presented to illustrate the possible impacts of an E3A wave on system voltages. A simple test system was provided to illustrate the methodology. Additionally, it was shown that the undesirable consequence of the E1/E2 waves tripping loads could potentially improve system stability, depending on the system characteristics, the amount of load shed, etc. Studying HEMP E3 in

transient stability enables the creation of more inexpensive mitigation strategies, such as configuring protection equipment for such a disturbance. It is clear that more detailed modeling is necessary, however the level of detail is to be determined. The case used in this chapter could certainly be more detailed, but it provides enough insight to suggest more detailed models for utilities studying this phenomenon is needed.

CHAPTER 4

HEMP E3 WAVEFORM SENSITIVITY

The E3 field produced from a HEMP could be prone to slight variations due to various atmospheric conditions and weapon characteristics. As a result, studying the impacts of one specific field may be incomplete. In this chapter, slight variations to the IEC reference field are made in order to better understand the potential power system impacts and sensitivities to various geoelectric field characteristics. The results show that the system's response is the most sensitive to changes to the geoelectric field's magnitude.

The test case that will be subjected to the disturbances is an adaptation of the 20 bus GIC benchmark case found in [32]. The 20 bus case has been augmented to include dynamic models for the loads, generators, exciters, and governors. The case also has basic protection systems modeled in the form of over excitation limiters (OELs), load relays, generator relays, and line relays. The inclusion of the protection system in transient stability modeling for HEMP E3 analysis is vital to the dynamic response of the system. Frequency constraints on the system are imposed through the use of generator relays but are somewhat relaxed compared to typical frequency restrictions. The generator relays are configured to trip if the

frequency deviates beyond 3% for more than 5 seconds. Most of the load has been moved to a new 161 kV network, which has been added to the case. GIS information, as well as ac line parameter data has been added to the case in order to make it appropriate for GIC transient stability analysis [33]. A constant impedance load model is used for the entire load, throughout each simulation. Although it is not the focus of this chapter, it is possible that low-cost mitigation strategies could be developed by configuring protection systems appropriately for HEMP E3. A snapshot of the 42 bus system is shown in Fig. 13.

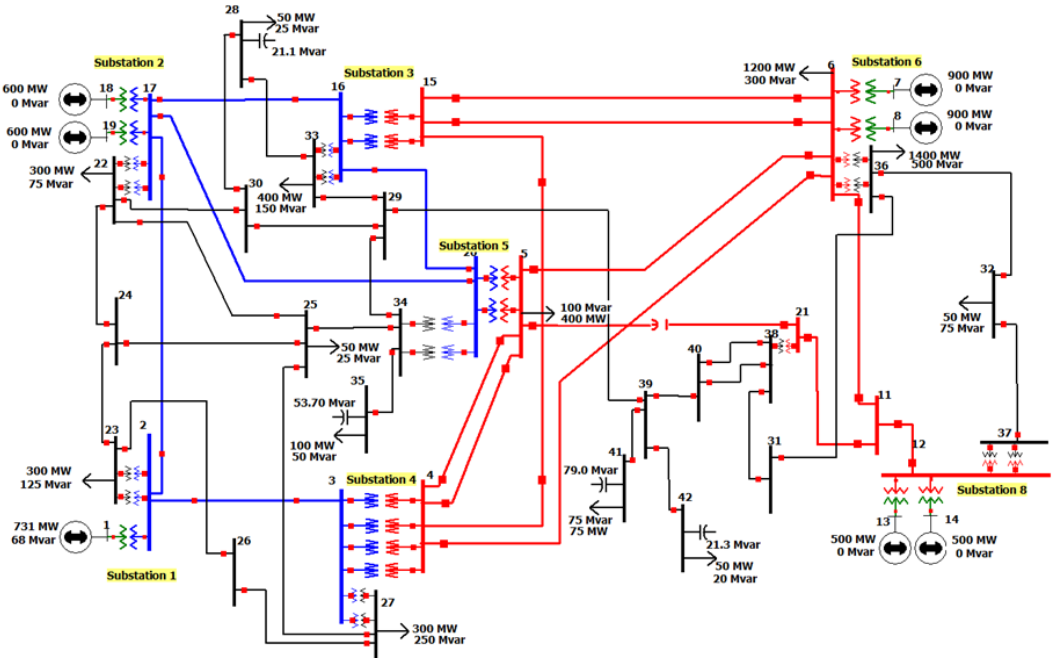

Fig. 13. The 42 bus test case

Four different potential HEMP E3 geoelectric fields were imposed on the 42 bus system. These fields were developed arbitrarily by slightly perturbing the

reference IEC field. The fields are shown in Fig. 14, and all assume a uniform ground conductivity.

1. IEC – reference HEMP E3 composite geoelectric field provided by the IEC
2. Fast Rise – geoelectric field is identical to (1) except the field rises four times as fast
3. Fast and High – geoelectric field rises and falls four times as fast and has an increased magnitude of 1.44 times (1)
4. Slow and Low – geoelectric field rises four times slower and reaches a peak magnitude of 0.625 times (1)

The IEC does not provide spatial data for the geoelectric field. In order to simulate the effects of the weapon's spatial distribution, each field was imposed on the system, scaled to 40%, 70%, and 100% of its peak field value.

It is very possible that the power network may lie in a region that is not in the most intense area of the geoelectric field. Depending on the blast location and altitude, it is possible that most power networks could be in regions that experience significantly attenuated geoelectric fields.

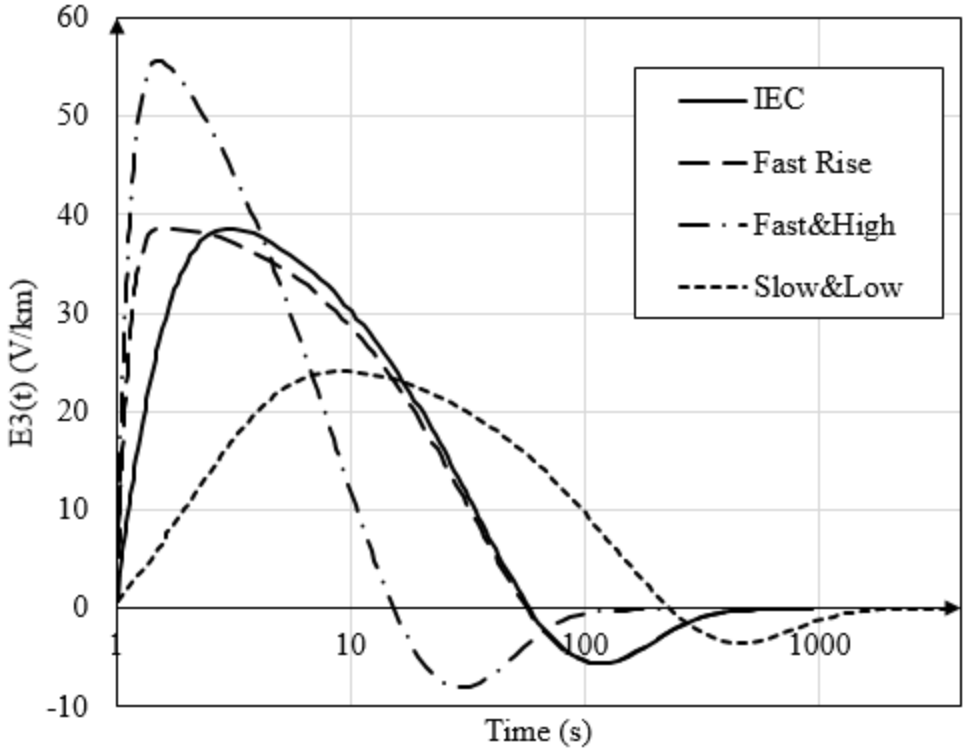

Fig. 14. Geoelectric fields used for simulations, 100% scaling

The area exposed to the 100% geoelectric field could be much less than the area exposed to less than 40% intensity [10]. It is also possible that large networks could span multiple areas of intensity. For this chapter, it is assumed the power network is small enough that it does not span multiple areas. In order to simulate the power network lying in entirely different geoelectric field intensity areas, the disturbances are scaled and separate simulations are run for each scaled disturbance.

The first 60 seconds of the IEC reference geoelectric field was applied to the test case. After the first 60 seconds, the field has negligible magnitude and is

not changing fast enough to significantly impact the system dynamics, therefore it is not simulated. The lowest bus voltage of the system response is shown for each geoelectric field intensity in Fig. 15. The system quickly collapses due to non-convergence for the 100% and 70% cases.

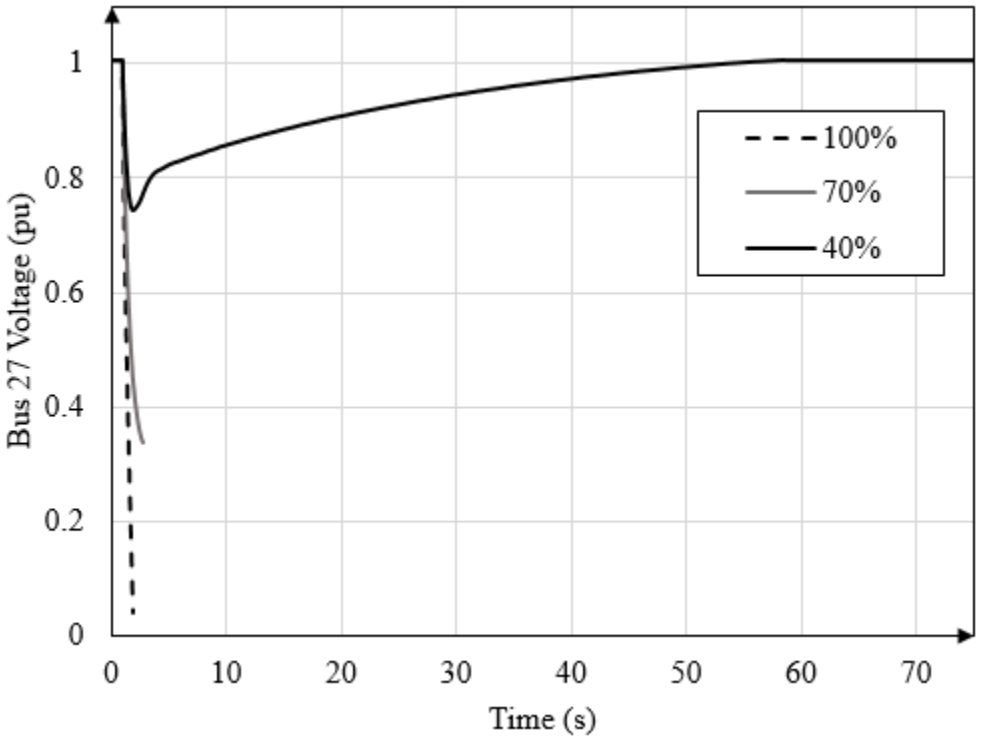

Fig. 15. System response to the IEC reference geoelectric field

The reactive power demand is too significant for the system to recover. Without change to the temporal evolution of the field, it is not surprising that the higher intensity fields negatively impact the power system more than the 40% field. The system recovers from the 40% intensity field without loss of load. The system

experiences a voltage drop, dipping as low as 0.745 pu. Protection systems did not trigger since the states did not violate any of the protection system settings.

A faster rising geoelectric field could pose as an increased threat to the short-term voltage stability of the power system. The fast rise field rises four times faster than the reference IEC field but decays at the same rate as the reference field. The simulation results are shown in Fig. 16. The faster rising field results in the system suffering a larger voltage drop at the most intense part of the disturbance, compared to that of the IEC reference scenario. The system fails in a similar fashion to that of the reference field for the 100% and 70% field intensity scenarios.

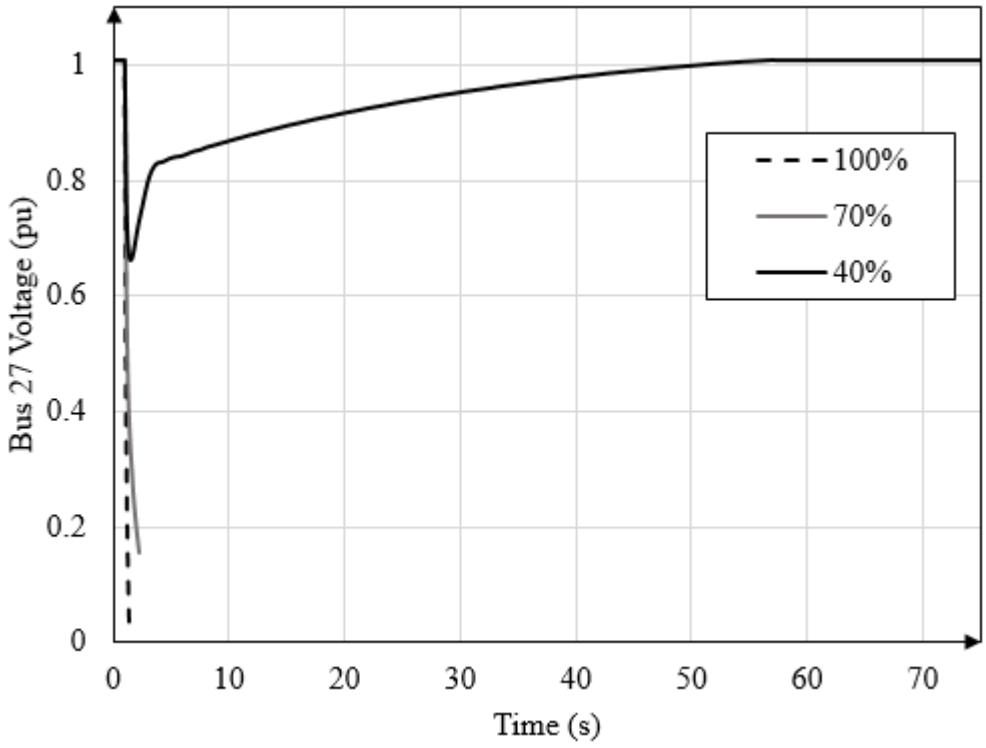

Fig. 16. System response to the fast rising geoelectric field

However, the 40% field intensity scenario recovers without the loss of any load, despite the disturbance's rise-time being four times that of the reference field.

The fast and high geoelectric field rises and falls four times as fast as the reference field. It also is larger in magnitude by a factor of 1.44. The fast and high disturbance lasts about 160 seconds with non-negligible magnitude, therefore the entire disturbance is simulated. The simulation results are shown in Fig. 17.

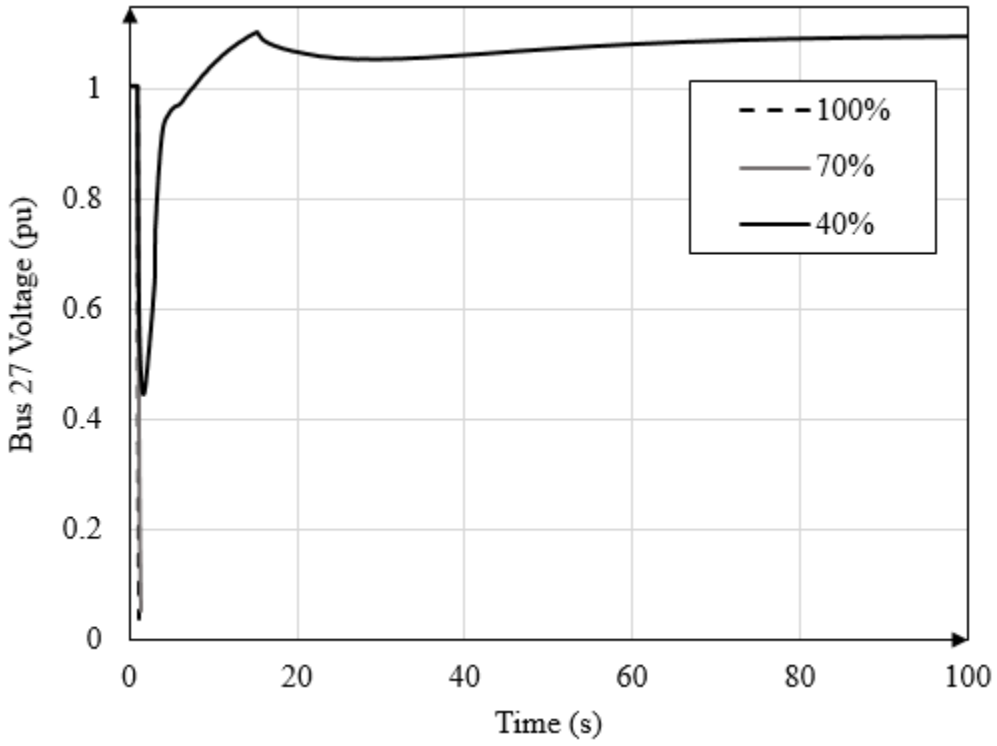

Fig. 17. System response to the fast and high rising geoelectric field

The fast and high geoelectric field had the most impact to the power system, at all levels of intensity, when compared to the other IEC perturbed fields. The 100% and 70% scenarios resulted in a non-convergence immediately as the

disturbance began. The system was able to maintain stability for the 40% scenario, however it did so by shedding load. The undervoltage load relays triggered on buses 5, 27, and 33 according to their relay settings of being lower than 0.75 pu for more than 2 seconds. Between 3.1 seconds and 3.129 seconds, 1230 MVA was shed, or about ¼ of the system load. After the load was shed, and the disturbance began to decay, and the system settled into a new steady-state operating point with slightly higher bus voltages, since ¼ of the load remained offline.

As expected, the slow and low geoelectric field had the least impact to the short-term voltage stability of the power system for all field intensity scenarios. The disturbance changes slowly enough that most of it is outside of the time response of the dynamics of the power system. However, the geoelectric field has a higher sustained geoelectric field than all of the others. The first 230 seconds of the geoelectric field was modeled into the simulations to catch any longer-term protection violations that would not have occurred for the other geoelectric fields. The simulation results are shown in Fig. 18.

The first protections system action performed in the 100% field intensity scenario is the opening of generator 18 by an overexcitation relay at 13.65 seconds. A few seconds thereafter, a series of loads trips, followed by the remaining generators tripping at 144 seconds. The sustained geoelectric field proved to be too great for the system to maintain convergence.

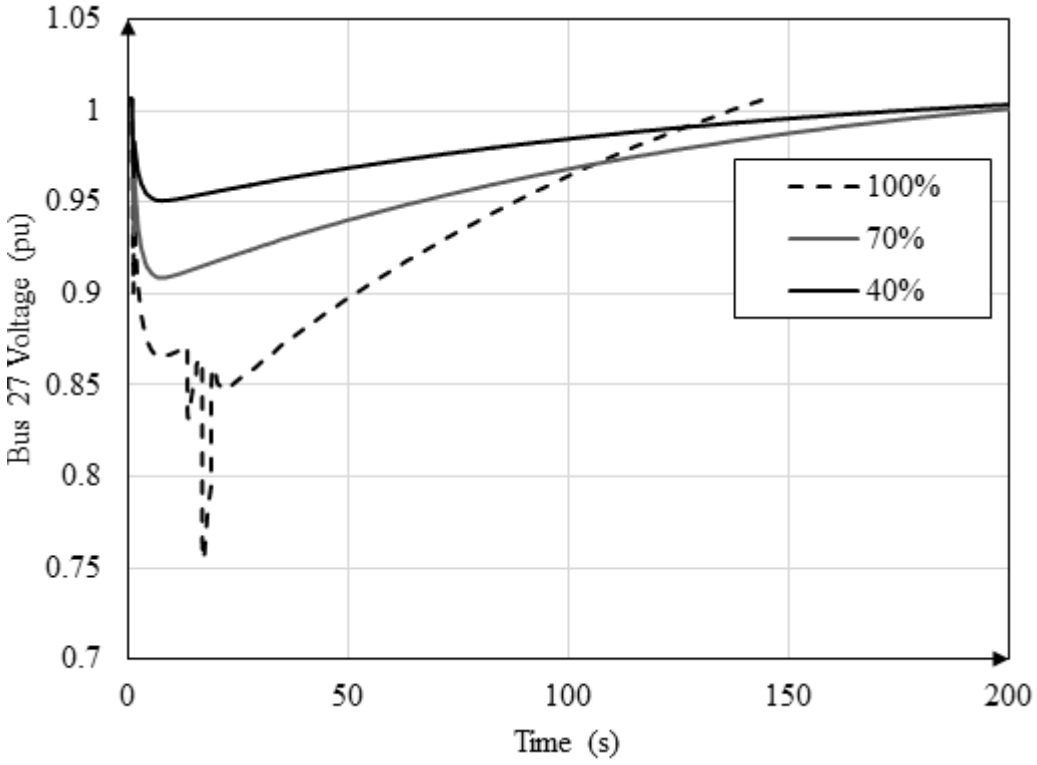

Fig. 18. System response to the slow and low rising geoelectric field

This is similar to how a system would fail due to a GMD, in the sense that the system cannot keep up with the additional load over time [28]. For the 70% intensity scenario, the lowest experienced voltage was 0.84 pu, no load was tripped, and the system returned to its original operating point. It should be noted that even though no load was shed, the system voltages were depressed longer than any of the other reference field perturbations. The system response to the 40% intensity scenario was very similar to that of the 70%. The 40% intensity scenario experienced a voltage as low as 0.92 pu. The slow and low field scenarios were the most forgiving to the system dynamics. Since the fields varied so slowly, the

dynamics of the system were able to keep up with the changes imposed by the disturbances. Also aiding in the robustness of the system response, compared to the other field perturbations, was the lower field magnitude.

In order to directly compare the system responses to the various geoelectric fields more easily, the system responses to each 40% intensity field are shown together in Fig. 19.

The system responses to the fast rise and IEC reference field are very similar. The most unique system responses are the responses to the slow and low geoelectric field and the fast and high geoelectric field, pointing toward the observation that a change in geoelectric field magnitude greatly impacts the system response. This is also observed by comparing the system responses to different field intensities of a specific geoelectric field.

This chapter compared and studied the responses of a 42 bus power system subjected to potential HEMP E3 geoelectric fields. By applying perturbations to the IEC reference geoelectric field, sensitivities of certain field parameters were studied. It was shown that the system's response was most sensitive to changes to the geoelectric field's magnitude. Varying the rise and decay time of the field did impact the system response, but not to the extent that varying the magnitude did. How the system responds is very dependent on the dynamic models and protection system settings used in the power system model.

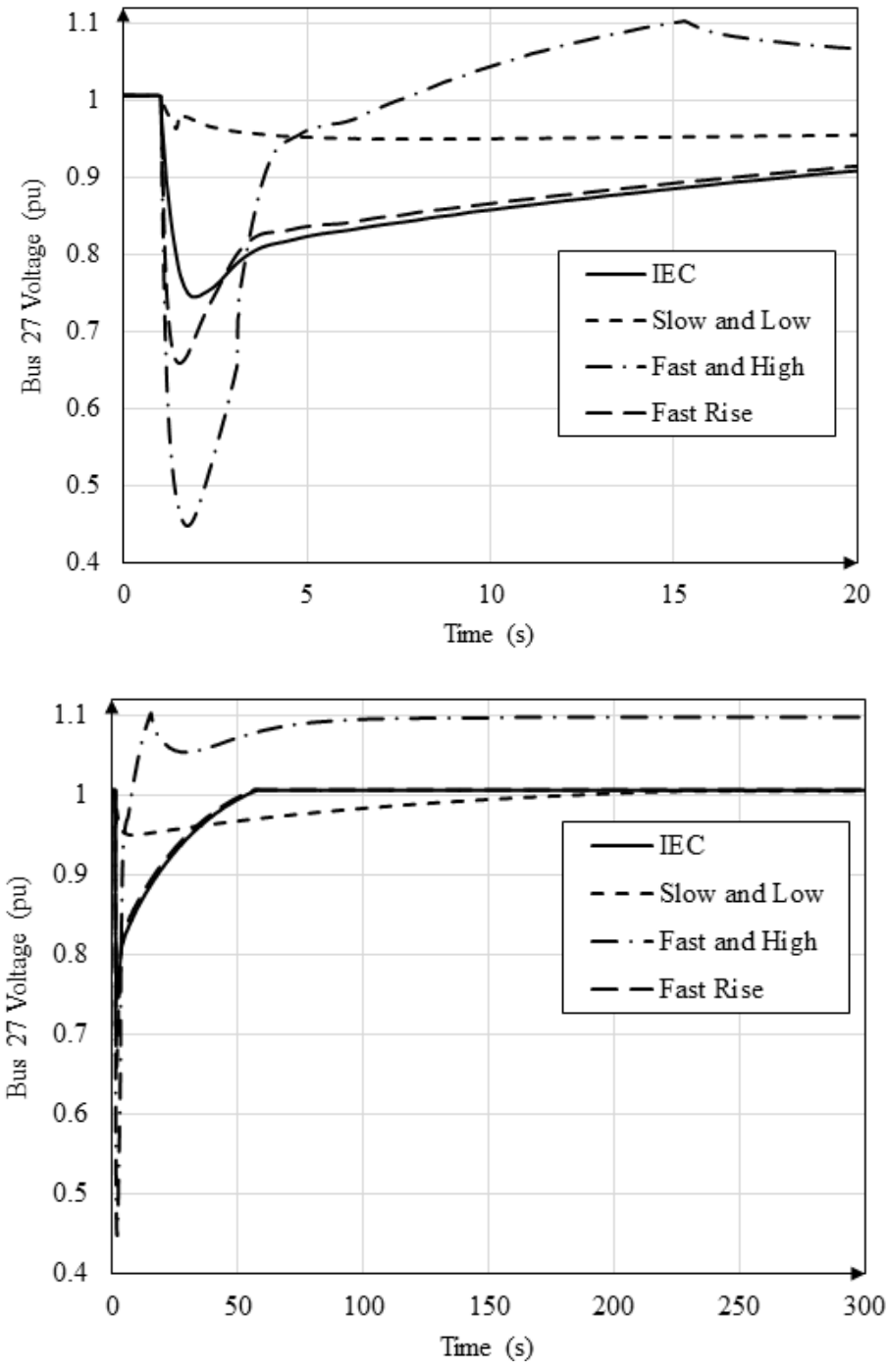

Fig. 19. Comparisons of the system response to 40% field intensities

The models and setting used in this chapter are popular choices in transient stability studies, with the exception of the relaxed frequency constraints. The impacts of E1 and E2 were not considered in this chapter. It is possible portions of the load would become damaged and drop before the E3 wave strikes, potentially impacting the dynamic response of the system.

One extension of this research could be studying how neighboring power systems contribute to voltage stability during HEMP E3 disturbances. Neighboring power systems may be in higher or lower geoelectric field intensity areas, hence contributing or distributing the burden of reactive power loading to the network of interest. Similar research has been performed in the GMD domain, studying how sensitive GICs for individual transformers are to the assumed geoelectric field on the transmission lines [25]. These large system studies present research challenges, such as modeling the spatial distribution of the geoelectric fields as well as the incorporation of ground conductivity models. Delivering software that is capable of simulating the effects of HEMP E3 to power systems to the hands of power system operators and planners is a crucial step in the hopes of mitigating the threat. Planners and operators intimately know their systems and can better create mitigation strategies.

HEMP E3 analysis belongs in the transient stability domain. Its faster rise-times, on the order of seconds, separates it from steady-state GMD analysis. This chapter focused on the voltage response of the system. The frequency response of

the system is also of importance, but not the focus of this chapter. One of the many challenges of incorporating HEMP E3 into transient stability analysis is identifying the appropriate load models. This chapter assumes a constant impedance load model for the load. In reality, the load has dynamics associated with it as well, but can be very power system dependent. Power system operators and planners would be able to characterize their load more appropriately when performing studies such as these in an effort to mitigate the risks associated with HEMP E3.

CHAPTER 5

ADVANCED GIC MODELING AND MITIGATION

Few academics study the GIC modeling and simulation problem. As a result, the research output over the years has been somewhat sporadic. Recently, however, there has been a surge in research, thanks to various regulatory agency task forces and utilities. As regulatory agencies begin to require certain levels of monitoring and protection against GIC, more advanced tools, data, and models are becoming available. This chapter focuses on the following three aspects of advanced GIC modeling: the time to saturation of transformers under dc current bias (GIC), impacts of transformer taping during HEMP E3, and non-uniform spatial distribution and ground conductivity models. The unique contributions of this chapter of the dissertation include taking existing advanced GIC models, improving/adapting the models for system studies, and performing/studying power system simulations with the improved, advanced models.

The test case used for the simulations in this chapter is the 42 bus Illini GMD test case, which was used in Chapter 4. However, the case has been improved by adding more realistic load models, protection system settings, and advanced GIC

modeling capabilities. Information on the load models and protection system settings can be found in Appendix C.

5.1 Time to Saturation of Transformers under DC Current Bias

A current subject of research in the area of GIC transformer saturation is determining the time it takes a transformer to saturate due to GIC, if any. In steady-state GMD analysis, this delay is of less importance since the analysis is performed in steady state, and thus the transformer is already saturated.

Research points toward a delay on the order of a few seconds. A delay on the order of a few seconds could potentially impact HEMP E3 analysis, significantly, since the time scale of concern is already on the order of seconds to minutes. Ultimately, the delay in saturation translates into a delay, and possibly mitigation, of reactive power consumption.

Assuming a delay does exist, the bigger question is how to model the delay. EMTP and finite element analysis were used in [24] to verify a delay model created for a specific transformer. The results indicate that the time to saturation is very dependent on the transformer's configuration, winding resistances, GIC level, and most of all, the core's magnetization characteristics. The magnetization curve was approximated to be piecewise linear. The time to saturation, $\Delta t(s)$, was found to be

$$\Delta t(s) = \frac{1}{2\pi f}\left\{\frac{V_g - V_0}{K_0} + 2.23\left[\frac{\bar{i}/I}{\sqrt{1-\bar{i}/I}}\left(\frac{V_0}{K_0}\right)^{1/2}\left(\frac{2\pi f\left(M_{sat}+L_p\right)}{R_p+3R_N}\right)\right]^{2/3}\right\}. \quad (15)$$

The following elements define (15): R_p is the total resistance in the primary circuit. R_N is the grounding resistance. L_p is the inductance in the primary circuit. M_{sat} is the magnetizing circuit's inductance, while in saturation. V_g is the peak phase to ground voltage that is required so that the transformer operates at the knee of its magnetization curve. V_0 is the peak phase to ground voltage. K_0 is the applied dc potential. $\bar{i}$ is the mean current that is reached while I is the final dc current.

This analysis is suitable for single transformers, but is not appropriate for large power system analysis where there are thousands of transformers with unknown characteristics. A key observation from [24] is that the delay length is dependent on the amount of dc excitation the transformer is experiencing. For high amounts of dc current, the delay is small, on the order of a few seconds. For small amounts of dc current, in the case most geomagnetic disturbances, the delay can be minutes long.

As a starting point, the delay can be simplified and generalized so that it can be applied to large-scale simulations. With the references indicating that the delay is on the order of seconds, a first-order lag delay was implemented in transient stability software. The delay is of the form $1/(s+T)$, where T is the user's desired delay in seconds.

To demonstrate this capability, a constant geoelectric field was applied to a power system with the time to saturation delay set to 1.0 seconds. A random transformer was observed during the simulation, the results are shown in Fig. 20.

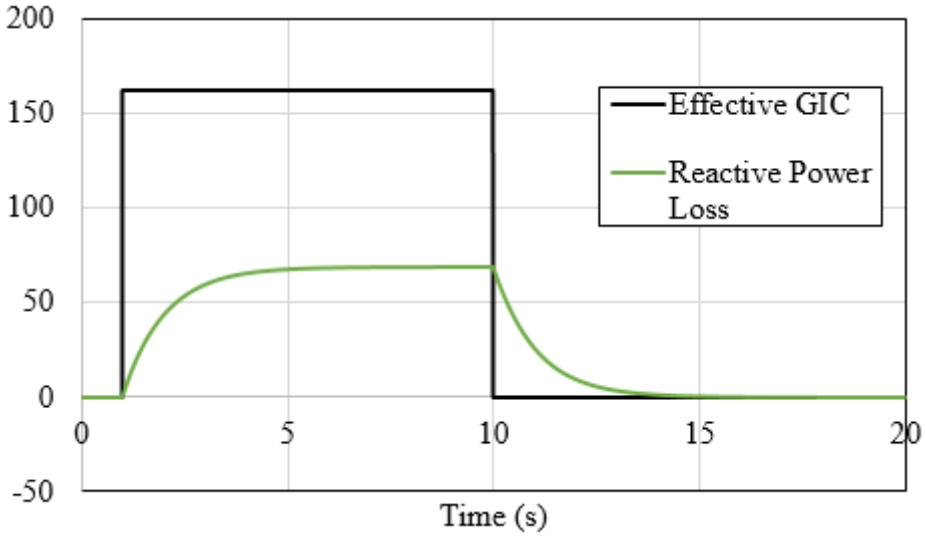

Fig. 20. An example of a transformer saturation delay

The delay takes the form of an exponential decay, e^{-Tt}, in the time domain. This theory was applied to the 42 bus test case shown in Fig. 13.

The purpose of the following simulations is to determine generally how the time to saturation impacts the power system response. It is expected that the saturation delay will dampen the transient response of the system. Three scenarios were imposed on the system, (1) no saturation delay, (2) 2 second saturation delay, and (3) 10 second delay. The power system was exposed to the IEC HEMP E3 waveform at 40% intensity. The system load was modeled as 20% MOTORW with the remaining 80% being split 75% constant impedance and 25% constant power. The voltage profile of the lowest bus voltage is shown for each scenario in Fig. 21.

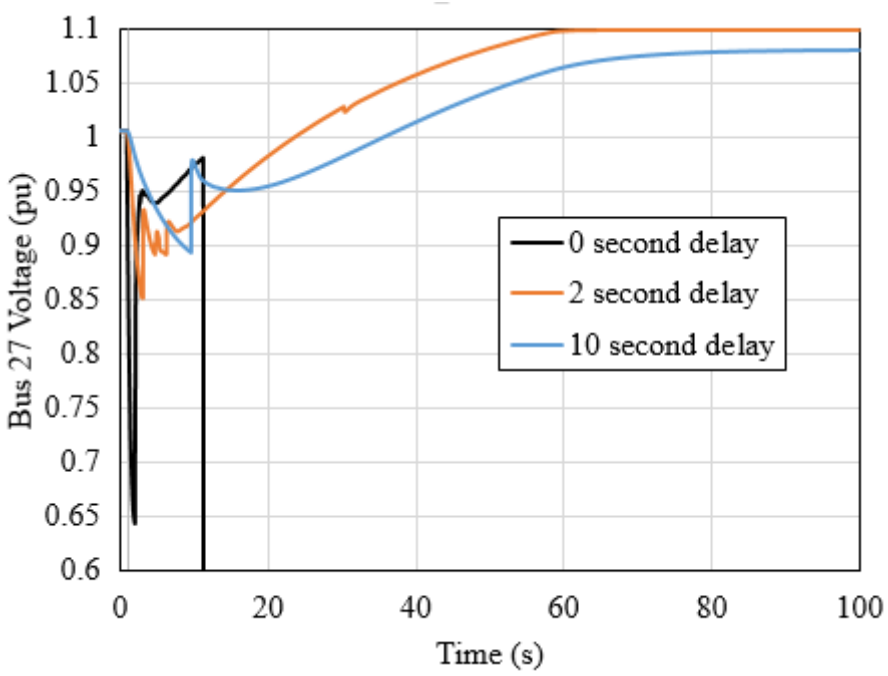

Fig. 21. System responses to various saturation delays

The 0 second delay scenario impacts the system the most drastically. The increased reactive power loading begins instantaneously as the disturbance evolves, yielding the worst-case scenario. All the load was shed followed by a complete system collapse.

For the 2 second delay scenario, the system is able to recover, but not without significant loss of load. The 2 second delay in saturation results in a delay in reactive power consumption during the initial rise of the HEMP E3 field. Buses 23, 27, 32, 33, 35 and 41 shed their combined load of 1225 MW (675 Mvar).

The system reaches its new operating point much slower as the delay is increased. The delay not only affects the transformer core's time to saturation, but

also its time to desaturation. The disturbance has already been decreasing for five seconds before the reactive power consumption begins for the 10 second delay scenario. The entire rise and initial fall of the transient has been excluded from the reactive power consumption calculations. As a result, the scenario experiences the least loss of load, 300 MW (250 Mvar).

Some of the system voltages reach a new steady-state operating point as high as 1.2 pu. This would obviously trigger overvoltage protection equipment. The takeaway, however, is that the saturation delay increases the system stability by mitigating the transient response induced by HEMP E3. System frequency is also of concern during these transients, but is not as significantly impacted by the saturation delay, due to the system inertia. The effects of the saturation delay are most easily observed through the system voltage response, hence it is shown here.

Certainly, improvements can be made to the delay model suggested in this dissertation. This model serves as a starting point as more data and research is made available, regarding transformer GIC saturation. The first 10 seconds during HEMP E3 are the most violent, if that part of the transient can be reduced, a significantly healthier system response can be obtained.

5.2 Impact of Transformer Tapping During HEMP E3

Transformer tapping is another power system dynamic that occurs in the seconds to minute timeframe. It is not always included in transient stability

modeling, however, its temporal domain overlaps with HEMP E3 analysis. More on how tap changing affects voltage stability can be found in [34].

A tapped transformer is a transformer that has the ability to regulate one side of the transformer's voltage by adjusting the turns ratio slightly. The adjustment of the turns ratio is an automatic, mechanical process. To prevent excessive tapping, a tapping delay on the order of 30 seconds is usually embedded in the tapping process. The turns ratio is incrementally changed in discrete steps. Each step can take on the order of a few seconds to fully change. Taps were added to a number of transformers in the 42 bus test case, previously mentioned. The transformers are configured to begin tapping once the respective low side bus voltage increases above 1.08 pu or decreases below 0.96 pu. The taps have a maximum and minimum regulation potential of 1.1 pu and 0.9 pu, respectively.

Two tapping scenarios were simulated and compared, slow tapping and fast tapping. The slow tapping scenario is configured so that there is a 30 second delay before the transformer begins to change its tap setting and when it first senses it should be changed. The tap is configured to step incrementally in 2 seconds. The fast tapping scenario has only a 2 second delay between sensing and changing the tap. It takes the tap 1 second to change one discrete step in the fast tapping scenario. The lowest bus voltage profile is shown for each scenario in Fig. 22.

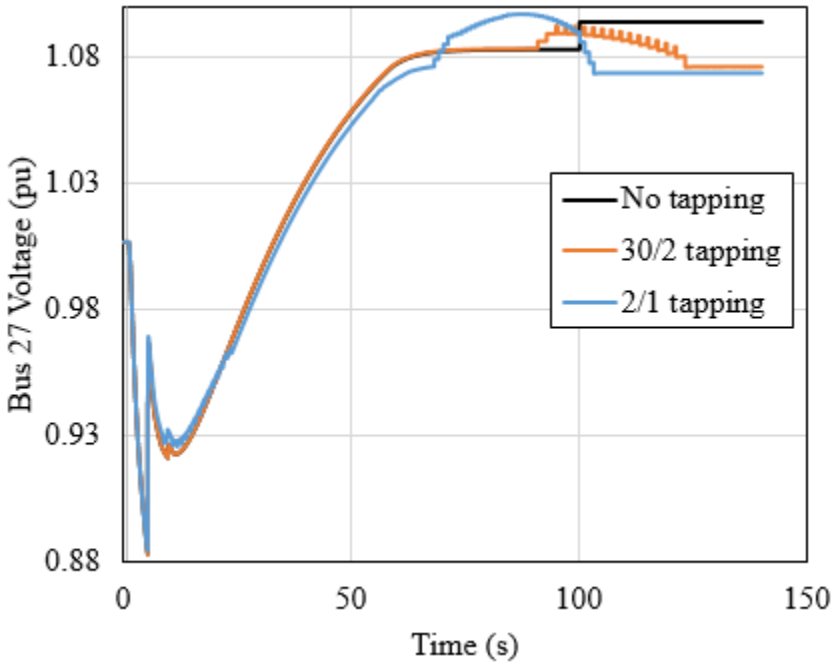

Fig. 22. Transformer tapping voltage profiles

Due to the delay on the two different tapping scenarios, the tapping does not significantly impact the fast dynamics during the initial rise of the disturbance. The tapping is most apparent as the system reaches its new steady-state operating point near the end of the simulations. The tap settings can be configured a number of ways, this is just a few examples of how changing the tapping delay affects the system response. The slow tapping scenario is not able to begin tapping until about the 90 second mark in the simulation since the voltage regulation bounds are not exceeded for a minimum of 30 seconds until then. The fast tapping was able to begin regulating the voltage much quicker since the minimum violation time to

begin tapping was much shorter. The tap changing of a transformer connecting buses 20 and 5 is shown in Fig. 23.

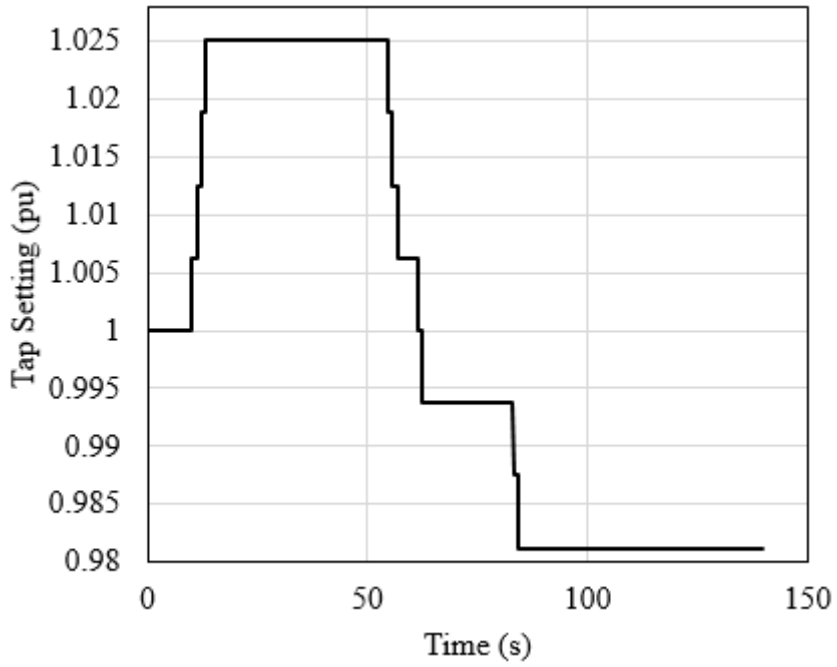

Fig. 23. Transformer 20-5 tapping

As expected, the tapping begins very quickly and is able to increase the bus voltages early on in the simulation. The transformer is set to its maximum tap setting for nearly 40 seconds before it begins to decrease as the disturbance decreases. The tap does not return to its original value. Since load was shed, the tap decreases in order to bring the system voltage back to a nominal level. Regulating the bus voltages is obviously desirable while attempting to maintain voltage stability. However, it may be also desirable to let the voltages fluctuate more than a normal tapping scheme would allow, in order to maintain frequency stability. For

example, if a large portion of the load is heavily voltage dependent, like a constant impedance load, and the system is at or near maximum loadability, maintaining the bus voltages and not letting them decrease to an "acceptable" level could result in load shedding, impacting the frequency stability of the system. If configured appropriately it is possible that transformer tapping can be used to mitigate disturbances like HEMP E3.

5.3 Non-Uniform Spatial Distribution and Ground Conductivity Models

Integrating HEMP E3 into steady-state power flow analysis begins by calculating the induced GIC. However, it is useful to have a basic understanding of the electric field that drives these GICs. Borrowing from GMD analysis, the electric field is induced from the earth's perturbed magnetic field. Terrestrial-based magnetometers record the variations of the magnetic field, seen at the surface of the earth. The relationship between the electric field, E, and magnetic field, H, in the frequency domain, based on the plane wave method and layered earth assumption, is defined by the ground impedance function Z(ω) [35], [36].

$$E(\omega) = Z(\omega) H(\omega) . \tag{16}$$

The ground impedance is heavily dependent on frequency. The earth behaves as a large conductor, and the electromagnetic waves will penetrate the earth to different depths, depending on the frequency. A basic view of the layered earth is shown in Fig. 24.

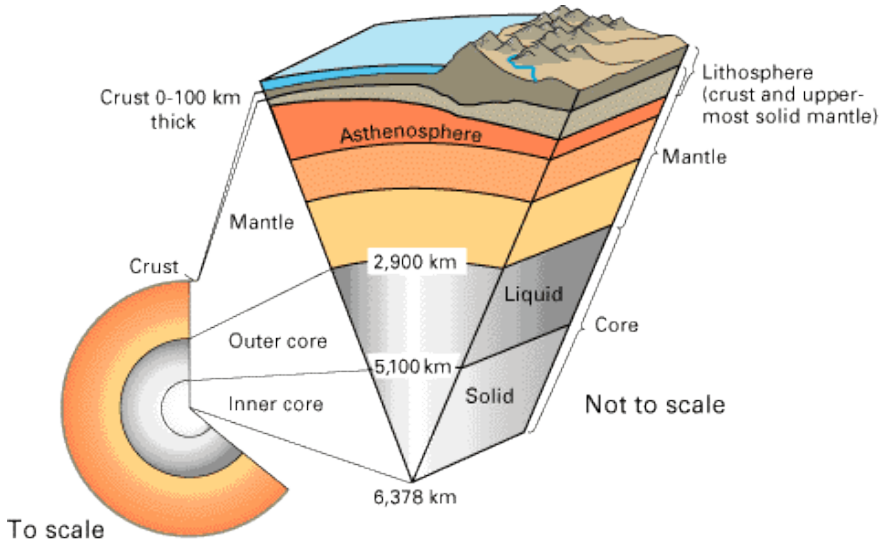

Fig. 24. Layered earth, from the USGS

The United States is divided into regions, each with a unique ground impedance structure. The regions, Fig. 25, are laterally uniform within the region. In other

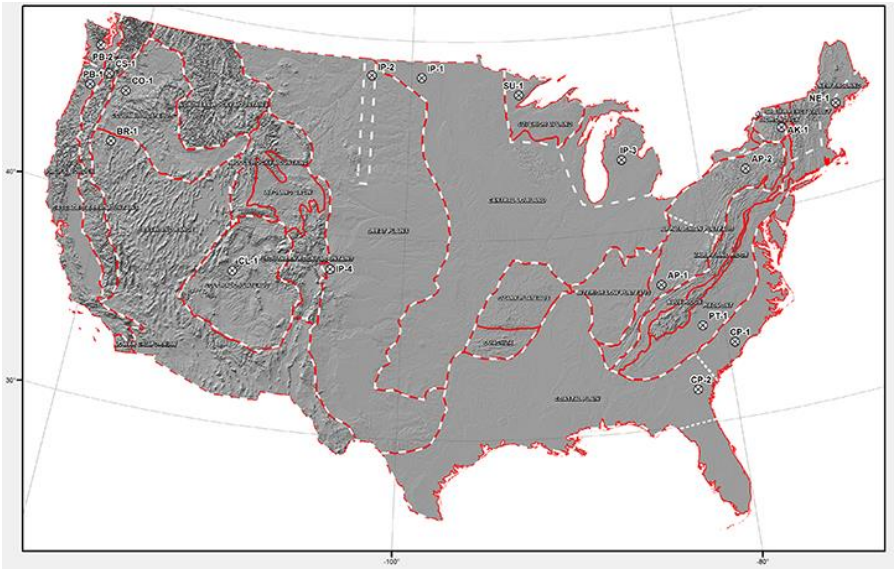

Fig. 25. Ground impedance regions for the United States, provided by the USGS

words, the impedance varies only with depth, in each region. The regions are modeled in piece-wise linear fashion, Fig. 26. A ground impedance model for the

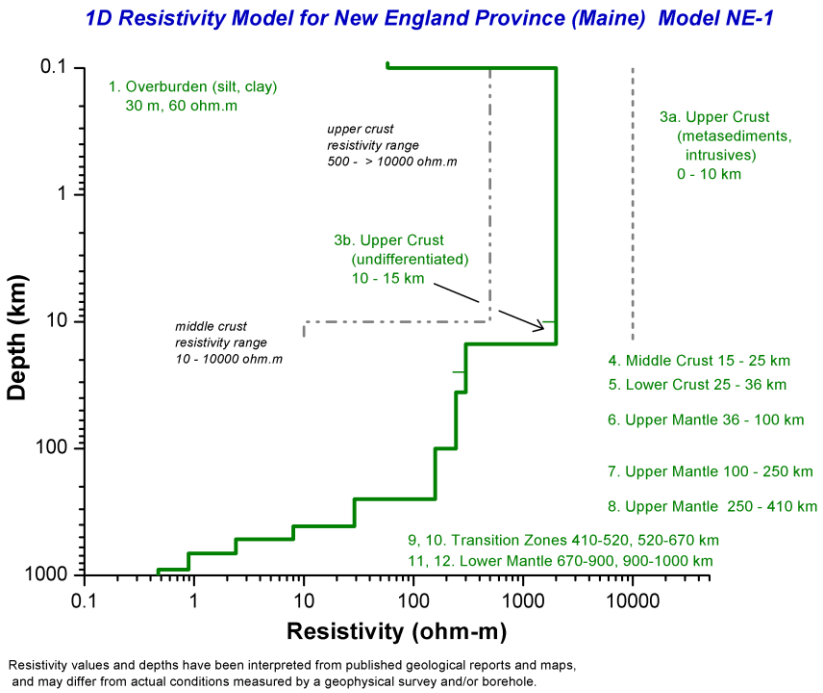

Fig. 26. Ground impedance structure of New England (Model NE-1), provided by the USGS

New England province is shown in Fig. 26. The general trend across the ground impedance regions is that the conductivity increases with depth. The ground impedance structure provides the data needed to calculate the ground impedance function $Z(\omega)$. The algorithm used for calculating $Z(\omega)$ is based off of [36], [37]. This method is verified by using magnetometer data taken during geomagnetic storms and comparing the calculated GICs from the magnetic fields.

The iterative procedure begins by first calculating the intrinsic impedance of the bottom-most layer, layer *n*.

$$Z_n(\omega) = \frac{E_n}{H_n} = \sqrt{j\omega\mu\rho_n}\ , \tag{17}$$

where E_n and H_n are the electric and magnetic field intensity, respectively, at layer *n*, *j* is the imaginary number, ω is the angular frequency, μ is the permeability, approximated as μ_0, and ρ_n is the resistivity of the n^{th} layer. The layers above the bottom layer need to account for each layer below itself by including the effects of the abrupt impedance changes at the boundaries between the each layer, as well as the layer depths. In general, the impedance at the i^{th} layer, except the bottom layer, is calculated as,

$$Z_i(\omega) = \left(\frac{1+\alpha_i}{1-\alpha_i}\right)\eta_i \text{ for i=n-1, n-2, ... , 1} \tag{18}$$

$$\alpha_i = \Gamma_{i+1} e^{-2\gamma_i \cdot \Delta h_i}$$
$$\Gamma_{i+1} = \frac{Z_{i+1} - \eta_i}{Z_{i+1} + \eta_i}$$
$$\gamma_i = \sqrt{\frac{j\omega\mu}{\rho_i}}$$
$$\eta_i = \sqrt{j\omega\mu\rho_i}$$
$$\mu = \mu_0,$$

where Δh_i is the i^{th} layer thickness, γ_i is the i^{th} layer propagation constant, and η_i is the intrinsic impedance of layer *i*. For an *n* layer earth model, (17) will be calculated first, and only once. Next, (18) is calculated a total of *n*-1 times, starting from the

lowest uncalculated layer, moving toward the surface. The final result is a function $Z(\omega)$, the total impedance seen at the surface for a given frequency, ω.

Next, the provided magnetometer data, $B(t)$, is transformed into the frequency domain using a fast Fourier transform (FFT), yielding $B(\omega)$. The magnetic flux density is then converted into magnetic field intensity, $H(\omega)$ and multiplied in the frequency domain with the impedance function to obtain the geoelectric field at the surface of the earth in the frequency domain, (16). Lastly, the inverse FFT is taken to obtain the geoelectric field seen at the surface of the earth in the time domain. This geoelectric field serves as input data for the calculation of GIC. Through this research, a tool was created in MATLAB which scrapes data in real time from the online magnetometers and calculates the induced geoelectric field at the desired location for GMDs. It is possible that this tool could be expanded to handle higher frequency disturbances that interact with the ground, such as HEMP E3.

Up to this point, the simulations used in this dissertation have assumed a uniform ground conductivity of 10^{-4} S/m and, unless otherwise noted, a spatial distribution factor of 40% intensity. This conductivity is suggested by the IEC and claims that the IEC HEMP E3 electric field scales as $1/\sqrt{\sigma}$. It should be noted that the frequency of which the IEC waveform is based on remains classified. The following simulation has non-uniform spatial distribution, as well as non-uniform

ground conductivity. The spatial and ground conductivity distributions are divided as shown in Fig. 27.

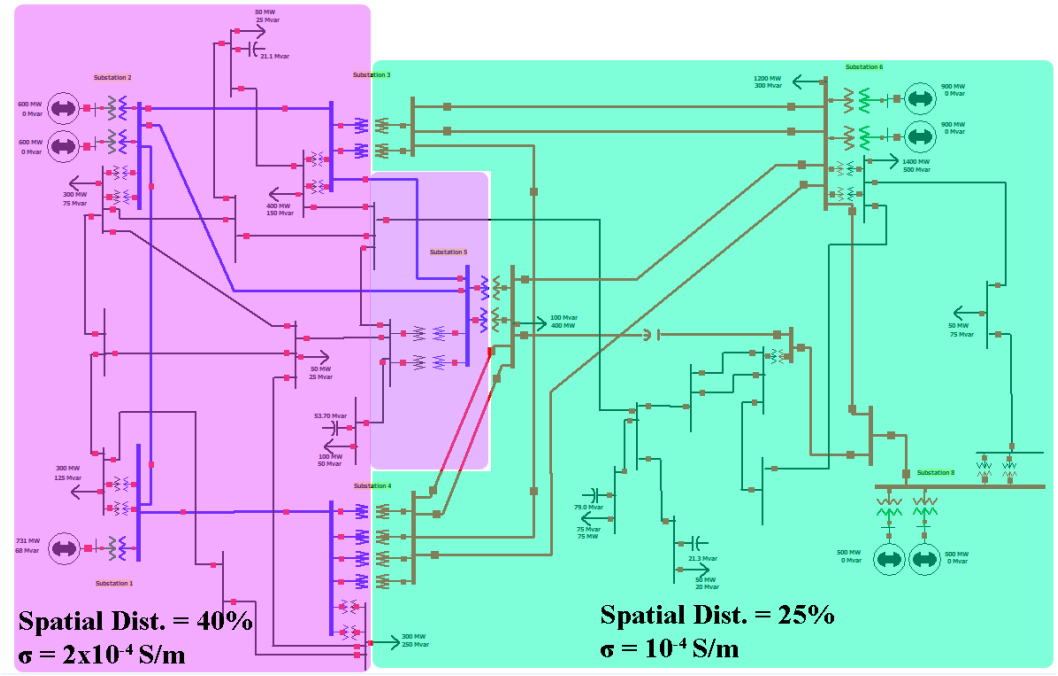

Fig. 27. Ground conductivity and spatial distribution mappings

The purple region in Fig. 27 exhibits a spatial distribution of 40% peak E3 intensity and a ground conductivity of $2x10^{-4}$ S/m, twice that of the IEC HEMP E3 field. The green region is characterized by a spatial distribution of 25% peak E3 intensity and a ground conductivity of 10^{-4} S/m. The two regions were chosen arbitrarily.

Doubling the conductivity effectively reduced the field intensity by a factor of 0.707 for the purple region. The combined intensity of each region can be seen by multiplying the spatial distribution factor times the ground conductivity factor,

resulting in a percentage of the IEC HEMP E3 field intensity. The purple region has an overall intensity of approximately 0.283 times the IEC HEMP E3 field and the green region has an intensity of 0.25 times the IEC HEMP E3 field. The simulation results, in the form of the lowest bus voltage profile, are shown in Fig. 28. The simulation uses a transformer saturation delay of 5 seconds. The transformer taps are set on a 15 second delay with 2 second tap change timing. In some sense, this simulation combines all of the modeling techniques developed thus far.

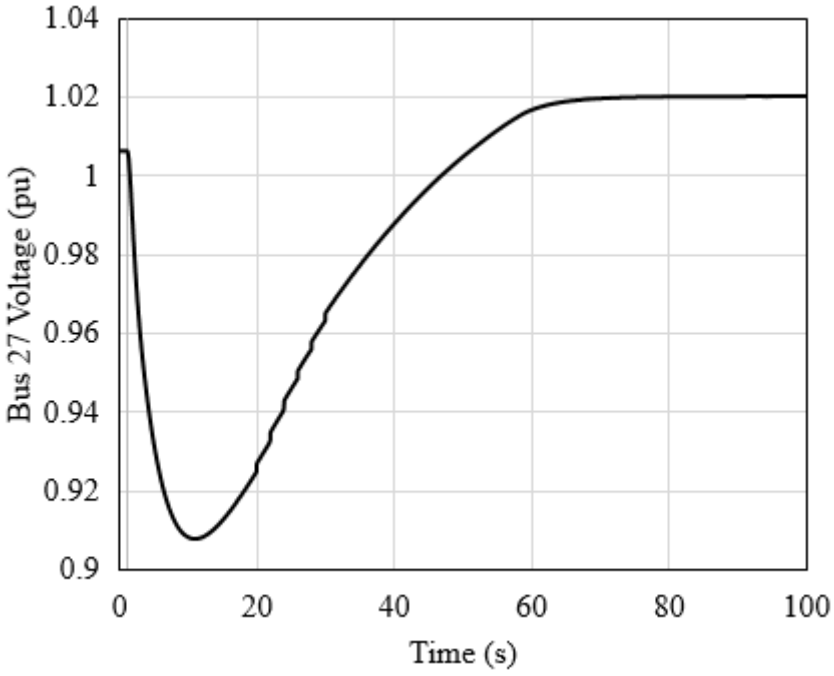

Fig. 28. Bus voltage for non-uniform ground conductivity and spatial distribution case

In this case, the chosen ground conductivities and spatial distributions lessened the severity of the disturbance to a level in which the system was able to

recover without the loss of load. If the ground conductivity is halved, instead of doubled in one region, the intensity factor increases by a factor of $\sqrt{2}$ and the system quickly collapses. The system responses can be highly dependent on the spatial and ground conductivity distributions. How the peak IEC HEMP E3 geoelectric field varies as a function of uniform ground conductivity is shown in Fig. 29.

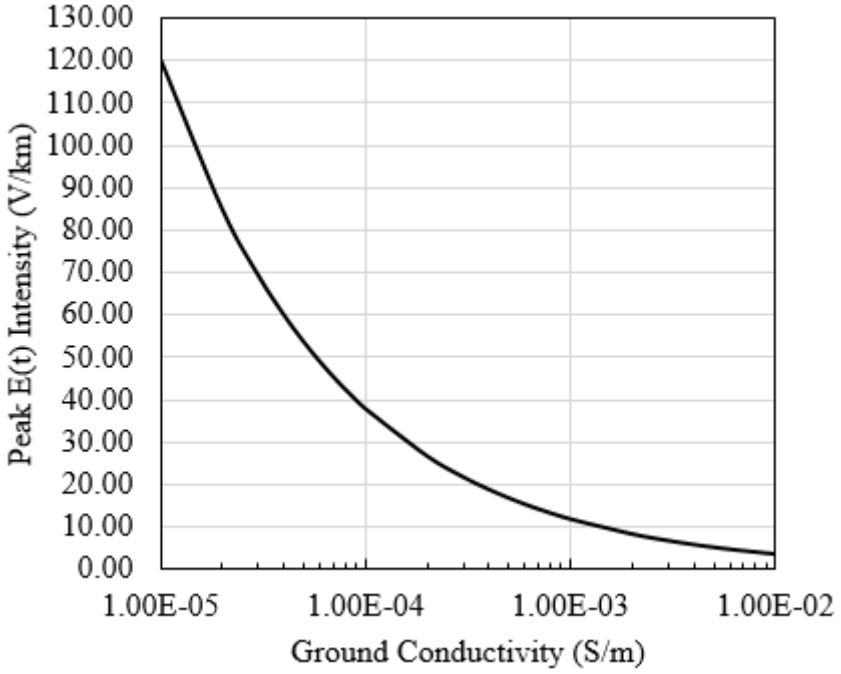

Fig. 29. Peak geoelectric field variation as a function of uniform ground conductivity

The overall geoelectric field intensity could take on an infinite value of intensities since the field is highly dependent on so many things. The scenario

shown in Fig. 27 is just one example. It should be noted that the frequency dependence of the ground conductivity has been ignored in this simulation.

In order to calculate the frequency-dependent non-uniform ground conductivities, magnetic field information regarding the disturbance must be obtained. Since the IEC does not disclose the magnetic field perturbations associated with the nuclear blast, it must be calculated from the provided geoelectric field and ground conductivity. A purely horizontal magnetic field is calculated according to

$$B(t) = \sqrt{\frac{\mu_0 \sigma}{\pi}} \int_0^t \frac{d\tau}{\sqrt{t-\tau}} E(\tau). \tag{19}$$

$E(t)$ is the electric field given by the IEC. The resulting magnetic field, $B(t)$, is shown in Fig. 30.

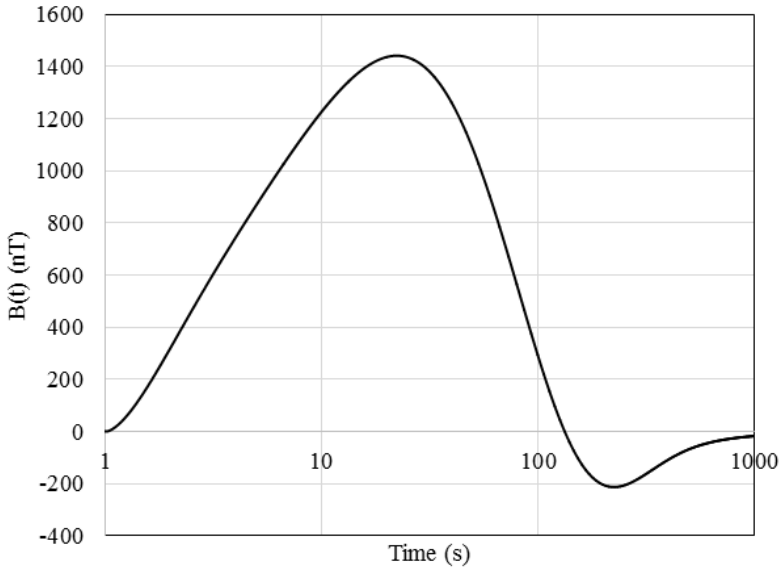

Fig. 30. The $B_3(t)$ reconstructed from $E_3(t)$

With the calculated magnetic field, new ground conductivity models can be applied and the induced geoelectric field can then be calculated as,

$$E(t) = \sqrt{\frac{1}{\pi \mu_0 \sigma}} \int_0^t \frac{dt'}{\sqrt{t - t'}} \frac{dB(t')}{dt'} \ . \tag{20}$$

Detailed assumptions and conditions for this procedure can be found in [10]. This method allows for frequency-dependent non-uniform ground conductivity models to be included into HEMP E3 analysis and has been verified for GMD analysis in [37] with GIC GMD data.

5.4 GIC Mitigation

Currently, mitigation techniques for GIC are focused on the strategic placement of GIC blocking devices [2], such as [38] by EMPrimus. In a simplistic view, these devices are effectively capacitors, installed in the neutral connection of wye-grounded transformers. The capacitors prevent dc current flow, while allowing ac current flow. This ensures a solid ground connection during fault conditions, while blocking GIC.

Adjusting the topology of the network is another form of mitigation. Topology control has been overlooked in the area of GIC mitigation. An example of topology control in the presence of E3 is presented here, on the 42 bus test case, using an interactive simulator.

Consider the 42 bus case used in Chapter 4, with the IEC HEMP E3 disturbance scaled to 40% of its original strength. The peak geoelectric field for

this disturbance is 15.5 V/km. The loads are modeled by 100% constant impedance. Without mitigation, the system experiences a frequency collapse around the 60 second mark, as seen in Fig. 31 and Fig. 32.

At 12.8 seconds, load 27 is tripped due to low voltage. At 21.4 seconds, the over-excitation limiter opens the relay to generator 8. At 60 seconds, the rest of the generators trip due to under frequency.

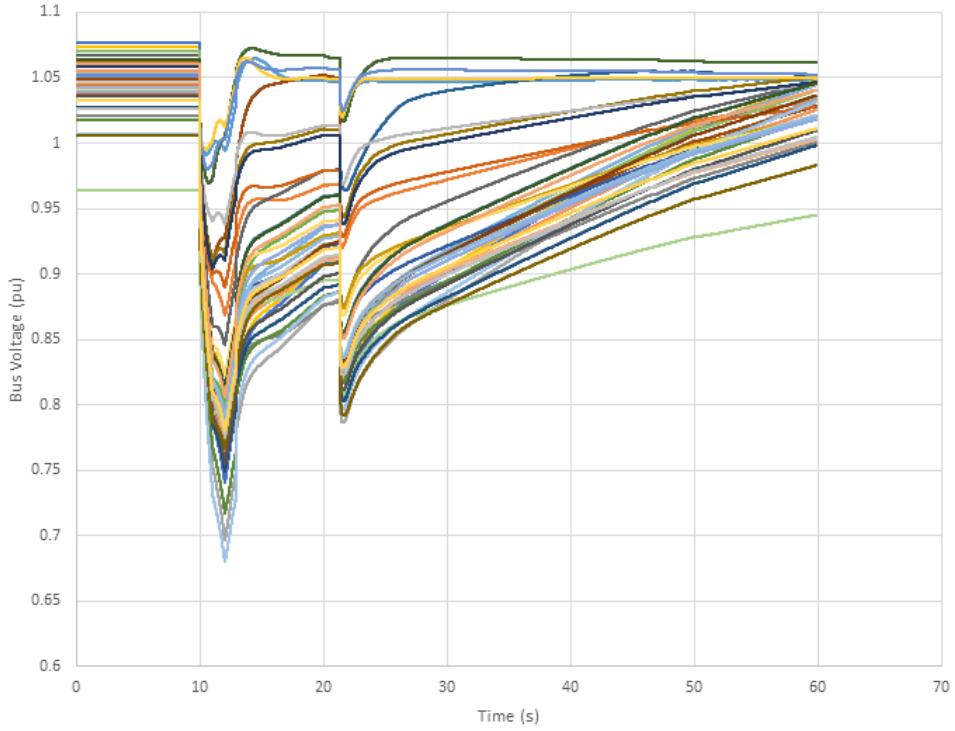

Fig. 31. Bus voltages in per unit for 42 bus case with no mitigation

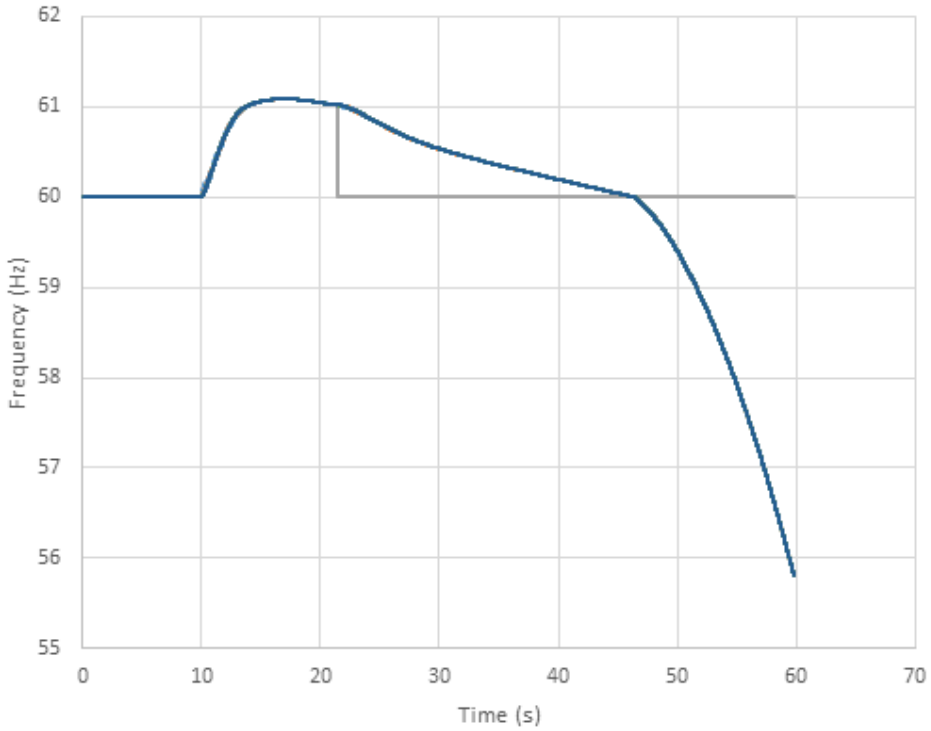

Fig. 32. Generator frequencies for 42 bus case with no mitigation

The following mitigation strategy is proposed to bring awareness to the mitigation issue. It is by no means optimized. The control actions taken, must be taken very quickly, perhaps much faster than an operator would be able to respond to the disturbance. However, as grid automation increases, a disturbance like this could be mitigated by automatic grid action.

Topology load control algorithms is a mitigation strategy which focuses on intelligent load switching. The decision to take mitigation action is based on the rate of change of voltage and frequency, as well as absolute voltage and frequency.

By controlling the load status, the dispatched power can attend to the saturated transformers, while the load is temporarily not serviced.

Intentional line outaging is also a viable option. Line outaging mitigates the effects of GIC by redirecting the flow of GIC. Also, outaging a line results in a reduction of GIC, since there will be no induced voltage on that line. One could imagine redirecting the flow of GIC toward areas of the system that have more available generation, or to more secure paths out of the system. When considering intentional outaging of a line, line length, GIC path, and local generation are key factors in the decision-making process.

The resulting voltage and frequency plots show the system fully recovering from the disturbance using load switching techniques, Fig. 33 and Fig. 34.

Load 6 is switched out at 12 seconds in an effort to keep the system frequency within tolerance. As the reactive power demand on the system decreases with E3, the load is switched back in at 50 seconds. The system resumes its original operation at nominal voltage and frequency.

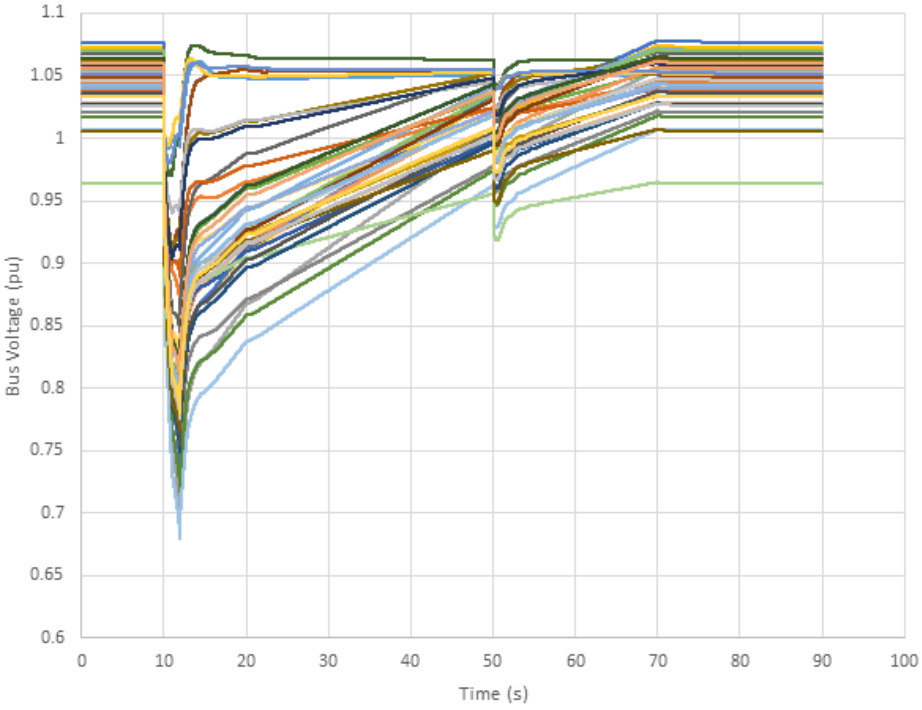

Fig. 33. Bus voltages for 42 bus case with load control mitigation

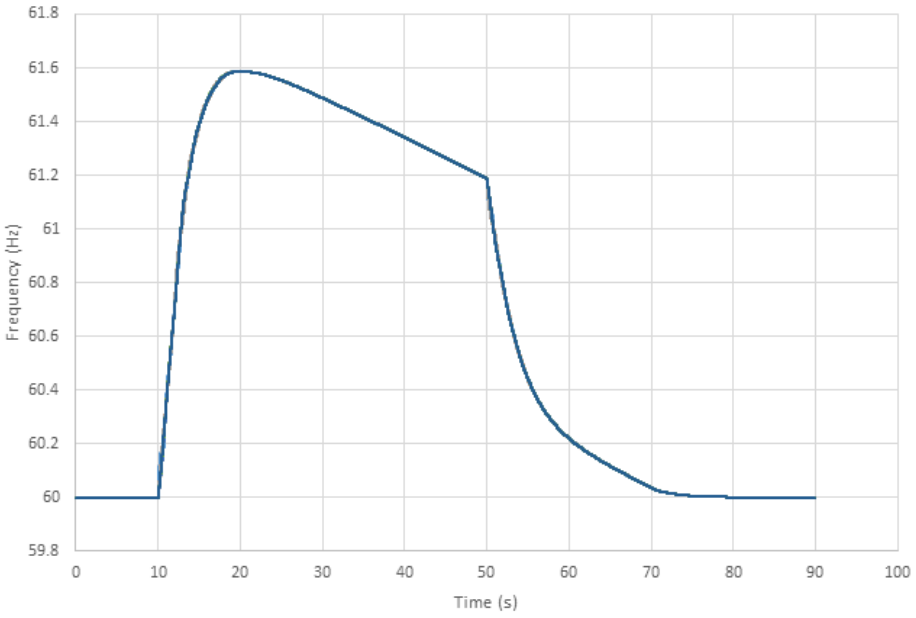

Fig. 34. Generator frequencies for 42 bus case with load control mitigation

Of all the available options for GIC mitigation, we believe topology control is the most promising. Of course, placing blocking devices on every GIC entry point could eliminate the GIC problem, it is not realistic for obvious reasons. Leveraging the existing infrastructure, like the protection system, to aid in topology control could significantly reduce the threat of GIC to a manageable level. Ultimately each power system is unique and behaves differently. That is why we recommended that power system operators and planners be at the forefront of creating mitigation strategies for their respective systems.

CHAPTER 6

CONCLUSION

This dissertation has developed models and tools in order to help characterize HEMP E3 impacts to power systems. Traditionally, many dynamics are not included in transient stability runs that are crucial in HEMP E3 analysis. Dynamics on the order of seconds to minutes are of prime influence. Power system responses can be very specific. Hence, the results can be very system dependent. That is why the intention of this research is to inform and equip power system operators and planners with models and tools encompassing the specific level of detail needed for HEMP E3 analysis.

A natural extension of this research is to increase the detail of the dynamic models used in the simulations. Load modeling, transformer saturation modeling, and protection system modeling, in many ways, are new to transient stability analysis. In particular, how to characterize a power systems load is an ongoing research topic that has major influence on transient stability results [29], [30], [31]. Including the protection system in transient stability analysis is becoming more popular. However, major questions remain about how the protection system should be configured in the simulations.

The modeling of a single transformer can be very unique. Slight differences in the core materials, windings, etc. can affect how transformers respond. There is significant room for improvement on understanding how high voltage transformers respond to dc current. Research topics such as transformer half-cycle saturation, even and odd harmonic generation, and reactive power consumption could play a major role in this research [18].

The studies performed in this dissertation involved relatively small systems, less than 42 buses. Since the HEMP E3 disturbance can be continental at scale, large system studies are encouraged, but will be met with their own challenges. This research primarily observed the voltage response of the simulated systems. The frequency response of the system is important and is certainly impacted by HEMP E3. Expanding the dynamic models beyond uniform frequency models could provide further insight into HEMP E3 analysis.

Ultimately, finding ways to mitigate the HEMP E3 threat is paramount. Mitigation strategies can lead to reactionary plans, like those for space weather events, which will aid the grid in its resiliency to such a threat [39]. Existing mitigation strategies for GMD induced GIC, such as GIC blocking devices, could play a role in HEMP E3 mitigation. Other techniques, such as topology control algorithms, [40], and protection system configurations have yet to be explored in depth for this application, but could yield promising results.

Modeling and simulation is a balance of detail and computation time. The codes written for this research were all run on an ordinary personal computer. As more data surrounding GIC becomes available, and the level of dynamic power system modeling increases, more meaningful results could be extracted from research in this field.

High impact, low frequency events pose a severe threat to the electric grid. While it may be unreasonable, or even impossible, to eliminate these threats entirely, it may be possible to mitigate them to a manageable risk. The ever increasing complexity of the grid leads to a less secure, more vulnerable, system. As the grid continues to grow, cyber and physical security should be of upmost importance to power system engineers.

APPENDIX A

PARAMETERS ASSOCIATED WITH THE 20 BUS GIC BENCHMARK CASE USED IN CHAPTER 3

This appendix lists the dynamic parameters used for the dynamic models associated with the 20 bus GIC benchmark case used in Chapter 3 of this dissertation. PowerWorld Simulator was used for the simulations.

TABLE A.1: MOTORW Parameters

Pul	0-.3	TV	30.0
Ls	3.6	Tbkr	0.0333
Lp	0.17	Acc	0.6
Ra	0.0068	Lpp	0.17
Tpo	0.53	Tppo	0
H	0.5	ndelt	10.0
D	2.0	wdelt	0.8
VT	0.6	Mbase	0.0

TABLE A.2: Transformer Series Reactance and Reactive Power Model (K Value)

Transformer	Series Reactance (pu)	K Value
T1	0.014	1.183
T2	0.025	1.163
T3	0.012	1.183
T4	0.012	1.183
T5	0.025	1.143
T6	0.011	0.816
T7	0.011	0.816
T8	0.025	1.163
T9	0.025	1.163
T10	0.015	0.816
T11	0.015	0.816
T12	0.025	1.163
T13	0.025	1.163
T14	0.025	1.163
T15	0.025	1.143

TABLE A.3: GENROU Parameters

H	3.0	Tdop	7.0
D	0.0	Tqop	0.75
Ra	0.0	Tdopp	0.035
Xd	2.1	Tqopp	0.05
Xq	0.5	S(1.0)	0.0
Xdp	0.2	S(1.2)	0.0
Xqp	0.5	Rcomp	0.0
Xdpp	0.18	Xcomp	0.0
Xl	0.15		

TABLE A.4: IEEET1 Parameters

Tr	0.0	Tf	1.46
Ka	50.0	Switch	0.0
Ta	0.04	E1	2.8
Vrmax	6.0	SE(E1)	0.04
Vrmin	-6.0	E2	3.73
Ke	-0.06	SE(E2)	0.33
Te	0.60	Spdmlt	0.0
Kf	0.09		

TABLE A.5: Transmission Line AC Parameters

From Bus	To Bus	Resistance (Ohm/m)	Reactance (Ohm/m)	Susceptance (Siemens/m)
2	3	3.511238	37.49288	641.5448
17	2	3.52314	36.89775	642.735
4	5	2.35	38.625	4125
4	5	2.35	38.625	0
4	6	4.675	76.875	8200
15	4	1.975	34.5	3500
5	6	2.975	44.5	6160
6	11	1.45	24.025	2542.5
15	6	2.925	48	5125
15	6	2.925	48	5125
11	12	2.325	40.75	4075
21	11	3.5	58.125	6180
16	17	4.66578	45.46755	849.8385
16	20	4.04685	41.4207	741.5258
17	20	6.939158	64.51155	1266.426

TABLE A.6: IEEEG1 Parameters

K	25.0	Uc	-10.0	T3	0.1	K1	1.0
T1	0.0	Pmax	1.0	Uo	1.0	All others	0.0
T2	0.0	Pmin	0.0	T4	0.1		

APPENDIX B

PARAMETERS ASSOCIATED WITH THE 42 BUS TEST CASE USED IN CHAPTER 4

This appendix lists the dynamic parameters used for the dynamic models associated with the 42 bus test case used in Chapter 4 of this dissertation. PowerWorld Simulator was used for the simulations. The case is available online [33]. The online version of the case, used in Chapter 4, contains the following parameters: AC lines, governors, generators, exciters, over-excitation limiters, transformers, governor relays, line relays, load relays, and component limits. The load in Chapter 4 was purely constant impedance.

APPENDIX C

PARAMETERS ASSOCIATED WITH THE 42 BUS TEST CASE USED IN CHAPTER 5

This appendix lists the dynamic parameters used for the dynamic models associated with the 42 bus test case used in Chapter 5 of this dissertation. PowerWorld Simulator was used for the simulations. This test case is extremely similar to the test case used in Chapter 4, with the following modifications: The load was 20% MOTORW with the remaining load split 75% constant impedance and 25% constant power. The load relays were adjusted to trip if the bus voltage dipped below 0.9 pu for more than one second. Shunt relays were added to the system, as well as LTCs with a step size of .00625.

TABLE C.1: MOTORW Parameters

Pul	0.2	TV	30.0
Ls	3.6	Tbkr	0.0333
Lp	0.17	Acc	0.6
Ra	0.0068	Lpp	0.17
Tpo	0.53	Tppo	0
H	0.5	ndelt	10.0
D	2.0	wdelt	0.8
VT	0.6	Mbase	0.0

TABLE C.2: LTC Transformers

From Number	To Number	Circuit
33	16	2
27	3	1
6	36	1
23	2	2
20	5	1
23	2	1
6	36	2
3	27	2
17	22	1
20	5	2
16	33	1
22	17	2
12	37	2
12	37	1

TABLE C.3: LTC Model (LTC1)

Tdelay	Tmotion
15	2

TABLE C.4: Shunt Relay (CAPRELAY)

Tfilter	0	t2On	0.5
tbClose	0.05	V1Off	1.2
tbOpen	0.05	t1Off	1
V1On	0.9	V2Off	1.15
t1On	1	t2Off	0.5
V2On	0.85		

REFERENCES

[1] "2012 Special reliability assessment interim report: Effects of geomagnetic disturbances on the bulk power system," NERC, February 2012.

[2] R. Neal, W. Radasky and J. G. Kappenman, "Developing an actionable EMP/GMD hardening program for an electric utility," in *2011 IEEE Power and Energy Society General Meeting*, 2011.

[3] C. L. Longmire, "On the electromagnetic pulse produced by nuclear explosions," *IEEE Transactions on Antennas and Propagation,* Vols. AP-26, no. 1, pp. 3-13, January 1978.

[4] Soviet Union, United Kingdom and United States, *Limited Test Ban Treaty,* U.S. Senate, 10 October 1963.

[5] *Electromagnetic compatibility (EMC) – Part 2: Environment – Section 9: Description of HEMP environment – Radiated disturbance. Basic EMC publication*, International Electrotechnical Commission, Geneva, Switzerland, IEC 61000-2-9.

[6] "Report of the commission to assess the threat to the United States from electromagnetic pulse (EMP) attack: Volume 1, executive report," 2004.

[7] "Report of the commission to assess the threat to the United States from electromagnetic pulse (EMP) attack: Critical national infrastructures," April 2008.

[8] K. W. Klein, P. R. Barnes and H. W. Zaininger, "Electromagnetic pulse and the eletric power network," *IEEE Transactions on Power Apparaturs and Systems,* vol. 104, no. 6, pp. 1571-1577, June 1985.

[9] A. K. Agrawal, H. J. Price and S. H. Gurbaxani, "Transient response of multiconductor transmission lines excited by a nonuniform electromagnetic field,"

IEEE Transactions on Electromagnetic Compatibility, vol. 22, no. 2, pp. 119-129, May 1980.

[10] Metatech Corporation, "The late-time (E3) high-altitude electromagnetic pulse (HEMP) and its impact on the U.S. power grid," Oak Ridge National Laboratory, January 2010.

[11] J. G. Kappenman and V. D. Albertson, "Bracing for the geomagnetic storms," *IEEE Spectrum,* pp. 27-33, March 1990.

[12] North American Electric Reliability Corporation, "Application guide: Computing geomagnetically-induced current in the bulk-power system," NERC, Atlanta, GA, 2013.

[13] V. D. Albertson, J. G. Kappenman, N. Mohan and G. A. Sharbakka, "Load-flow studies in the presence of geomagnetically-induced currents," *IEEE Transactions on Power Apparatus and Systems,* vol. 100, pp. 594-606, February 1981.

[14] J. G. Kappenman, "Geomagnetic storms and their impacts on the U.S. power grid," Metatech Corporation, Goleta, CA, January 2010.

[15] T. J. Overbye, T. R. Hutchins, K. Shetye, J. Weber and S. Dahman, "Integration of geomagnetic disturbance modeling into the power flow: A methodology for large-scale system studies," in *2012 North American Power Symposium*, Champaign, IL, September 2012.

[16] D. H. Boteler and R. J. Pirjola, "Modeling geomagnetically induced currents produced by realistic and uniform electric fields," *IEEE Transactions on Power Delivery,* vol. 13, pp. 1303-1308, October 1998.

[17] T. R. Hutchins, "Geomagnetically induced currents and their effect on power systems," M.S. Thesis, University of Illinois at Urbana-Champaign, Urbana, IL, May 2012.

[18] X. Dong, Y. Liu and J. G. Kappenman, "Comparitive analysis of exciting current harmonics and reactive power consumption from GIC saturated transformers," in *IEEE 2001 Winter Meeting*, Columbus, OH, January 2001.

[19] R. A. Walling and A. H. Khan, "Characteristics of transformer exciting current during geomagnetic disturbances," *IEEE Transactions on Power Delivery,* vol. 6, no. 4, October 1991.

[20] J. Berge, R. K. Varma and L. Marti, "Laboratory validation of the relationship between geomagnetically induced current (GIC) and transformer absorbed reactive power," in *IEEE Electrical Power and Energy Conference,* 2011.

[21] L. Marti, J. Berge and R. K. Varma, "Determination of geomagnetically induced current flow in a transformer from reactive power absorption," *IEEE Transactions on Power Delivery,* vol. 28, no. 3, July 2013.

[22] U. Bui, T. J. Overbye, K. Shetye, H. Zhu and J. Weber, "Geomagnetically induced current sensitivity to assumed substation grounding resistance," in *North American Power Symposium (NAPS),* September 2013.

[23] M. Lahtinen and J. Elovaara, "GIC occurrences and GIC test for 400 kV system transformer," *IEEE Transactions on Power System Delivery,* vol. 17, pp. 555-561, April 2002.

[24] L. Bolduc, A. Gaudreau and A. Dutil, "Saturation time of transformers under dc excitation," *Electric Power Systems Research,* vol. 56, pp. 95-102, 2000.

[25] T. J. Overbye, K. S. Shetye, T. R. Hutchins, Q. Qiu and J. D. Weber, "Power grid sensitivity analysis of geomagnetically induced currents," *IEEE Transactions on Power Systems,* vol. 28, no. 4, November 2013.

[26] P. W. Sauer and M. A. Pai, *Power System Dynamics and Stability,* Champaign, IL: Stripes Publishing L.L.C., 1997, p. 4.

[27] A. Pulkkinen, E. Bernabeu, J. Eichner, C. Beggan and A. Thomson, "Generation of 100-year geomagnetically induced current scenarios," *Space Weather,* 2012.

[28] T. J. Overbye, K. S. Shetye, Y. Z. Hughes and J. D. Weber, "Preliminary consideration of voltage stability impacts of geomagnetically induced currents," in *Power and Energy Society General Meeting (PES),* July 2013.

[29] WECC, "WECC approved dynamic model library," March 2015. [Online]. Available: https://www.wecc.biz/Reliability/Approved_Dynamic_Models_March_2015.pdf.

[30] IEEE Task Force on Load Representation for Dynamic Performance, "Load representation for dynamic performance analysis," *IEEE Transactions on Power Systems,* pp. 472-482, May 1993.

[31] IEEE Task Force on Load Representation for Dynamic Performance, "Standard load models for power flow and dynamic performance simulation," *IEEE Trasactions on Power Systems,* vol. 10, no. 3, pp. 1302-1313, August 1995.

[32] R. Horton, D. H. Boteler, T. J. Overbye, R. Pirjola and R. C. Dugan, "A test case for the calculation of geomagnetically induced currents," *IEEE Transactions on Power Delivery,* vol. 27, no. 4, pp. 2368-2373, October 2012.

[33] T. R. Hutchins, "Power dynamics scenarios: IlliniGMD 42 HEMP," [Online]. Available: http://publish.illinois.edu/smartergrid/illinigmd-42-hemp/. [Accessed 11 6 2015].

[34] C. C. Liu and K. T. Vu, "Analysis of tap-changer dyamics and construction of voltage stability regions," *IEEE Transactions on Circuits and Systems,* vol. 36, pp. 575-590, April 1989.

[35] J. R. Wait, *Wave Propagation Theory*, New York: Pergamon, 1981.

[36] W. C. Chew, *Waves and Fields in Inhomogenous Media*, New York: Wiley-IEEE Press, 1995.

[37] L. Marti, A. Rezaei-Zare and D. Boteler, "Calculation of induced electric field during a geomagnetic storm using recursive convolution," *IEEE Transactions on Power Delivery,* vol. 29, no. 2, pp. 802-807, April 2014.

[38] EMPrimus, "EMPrimus solid ground neutral DC blocking system," [Online]. Available: http://emprimus.com/emp-iemi_products/grid-and-transformer-protection.php.

[39] National Science and Technology Council, "National space weather action plan," Executive office of the President of the United States, Washington D.C., October 2015.

[40] P. A. Ruiz, J. M. Foster, A. Rudkevich and M. C. Caramanis, "Tractable transmission topology control using sensitivity anlaysis," *IEEE Transactions on Power Systems*, vol. 27, no. 3, pp. 1550-1559, August 2012.